Superconducting Nanowires Fabricated Using DNA and Nanotubes as Molecular Templates

Alexey Bezryadin[*†] and Paul M. Goldbart[‡§]

August 20, 2009

Abstract

The application of single molecules as templates for nanodevices is a promising direction for nanotechnology. In our research we use suspended deoxyribonucleic acid molecules or suspended single-wall carbon nanotubes as templates for making superconducting devices, and then study these devices at cryogenic temperatures. Because the resulting nanowires are extremely thin, i.e. comparable in diameter to the templating molecule itself, their electronic state is highly susceptible to thermal fluctuations. The most important family of these fluctuations are the collective ones, which take the form of Little's phase slips, or ruptures of the many-electron organization. These phase slips break the quantum coherence of the superconducting condensate, and render the wire slightly resistive (i.e., not fully superconducting), even at temperatures substantially lower than the critical temperature of the superconducting transition. At low temperatures, for which the thermal fluctuations are weak, we observe the effects of quantum fluctuations, which lead to the phenomenon of macroscopic quantum tunneling. In devices having two parallel nanowires, we find resistance oscillations with magnetic field. Such oscillations are a manifestly quantum-mechanical phenomenon that reflects the sensitivity of the supercurrent to the electromagnetic vector potential. The modern fabrication method of molecular templating, reviewed here, can be readily implemented to make nanowires from other materials, such as normal metals, ferromagnetic alloys, and semiconductors.

[*]Frederick Seitz Materials Research Laboratory and Department of Physics, University of Illinois at Urbana-Champaign, Urbana, Illinois 61801, U.S.A.

[†]bezryadi@illinois.edu

[‡]Frederick Seitz Materials Research Laboratory, Institute for Condensed Matter Theory, and Department of Physics, University of Illinois at Urbana-Champaign, Urbana, Illinois 61801, U.S.A.

[§]goldbart@illinois.edu

Keywords: nanofabrication, superconducting nanowire, DNA, molecular template, MQT.

1 Introduction

Deoxyribonucleic acid (DNA) contains genetic instructions used in the development and functioning of living organisms. The main function of DNA is to store information over long periods of time, thus the molecule has to be very robust. Chemically, DNA consists of two long polymers composed of simple units called nucleotides and forming the well-known Crick-Watson double helix,[1] the diameter of which is $\sim 2\,\mathrm{nm}$.

A new field, known as DNA nanotechnology, has emerged recently. It relies upon the unique molecular recognition properties of DNA molecules to create self-assembling DNA constructs having useful properties.[2] DNA is thus being used as a *structural template*, rather than as a carrier of biological information. Such an approach has been used to create a great variety of two-dimensional periodic patterns and networks, as well as three-dimensional constructs in the shapes of polyhedra.[3] The templating functions of DNA have been demonstrated in recent experiments in which a linear arrangement of nanoparticles, such as gold nanoclusters or streptavidin proteins, was achieved on the surface of the DNA molecule.[4] It is becoming evident that DNA can be regarded as a "backbone" for the fabrication of information-processing devices, chemical and biological sensors, and molecular transistors at the nanometer-size scale.[5,6]

By taking advantage of DNA self-assembly capabilities,[7] one can envision using single DNA and/or self-assembled DNA constructs as scaffolding for the

creation of metallic or even superconducting networks of wires. In fact this potential of DNA self assembly is the main reason why our work on metal coating of DNA was started. The approach could lead to creating of complex metallic networks with the smallest dimensions of the order of the diameter of DNA. The key to practical realizations of DNA molecular templating lies in the possibility of creating a homogeneous metal coating on single molecules, which transforms the molecules into thin metallic wires. In the first such attempts, a wet-chemistry approach was used to metallize DNA.[8–11] This approach tends to yield rather granular wires, which typically exhibit very high electrical resistance at low temperatures. These two problems (granularity and very high resistance at cryogenic temperatures) are in fact related to each other. If the wire is composed of weakly connected metallic grains, electrons tend to localize on these grains, due to the Coulomb blockade effect.[12–14] This effect leads to a strong increase of the electrical resistance as, at low temperatures, individual electrons have great difficulty passing from one grain to another. This is because the metallic grains are so small that the addition of even a single extra electron on a grain strongly increases the energy. This additional energy required for a current to flow through an inhomogeneous nanowire is not available at low temperatures, for which thermal fluctuations are negligible. Thus, the main goal in the development of the molecular templating technique amounted to finding a way of making homogeneous wires, so that the electrons in these wires could flow freely through them.

Molecular templating (MT),[15] which is a physical rather than a chemical method, offers the possibility of fabricating homogeneous wires, which can be made very short (as short as $\sim 30\,\mathrm{nm}$)[16] and very thin, viz. as thin as $\sim 5\,\mathrm{nm}$ or possibly even thinner.[15,17–20] The MT technique involves the sputter-deposition of

a thin metallic film over suspended (and dried) DNA molecules[18,21,22] or a carbon nanotubes.[15,17,19] The results published so far indicate that not all metals form homogeneous nanowires when deposited on the surface of a carbon nanotube. Amorphous alloys, such as $\mathrm{Mo}_x\mathrm{Ge}_{1-x}$, provide wires having a high degree of homogeneity.[15,20] For pure metals the general tendency is to form disconnected grains when deposited on a carbon nanotube.[17] On the other hand, some elemental metals, such as Nb,[19,23] amorphous Os,[19] and Ti,[17] exhibit strong adhesion to the nanotube. These metals can be used as "sticking" layers for other metals.[17] Thus, in the MT method the choice of the material determines the morphology of the resulting nanowire. In this Progress Report we focus on wires made by a sputter-deposition of $\mathrm{Mo}_{79}\mathrm{Ge}_{21}$ films[24,25] over suspended carbon nanotubes or DNA molecules. The elemental compositions of the alloy were as indicated (or similar to this), and were optimized with the goal of obtaining the highest critical temperature for the superconducting transition. This particular alloy shows an excellent adhesion to nanotubes and to DNA. The MT method also has the virtue of creating wires that are seamlessly connected to the measurement leads. Thus, the MT technique provides an efficient solution to the general problem of making good electrical contact to the nanowires under investigation.

Two types of experiments have been conducted on superconducting nanowires, viz. measurements on single wires and ones on double-wire quantum interference devices. Single-wire devices are used to study quantum coherence and decoherence effects in one-dimensional (1D) superconductors. A single-wire device consists of two macroscopic superconducting films (to be called "electrodes" or "thin film electrodes"), connected electrically to each other through just one individual superconducting nanowire. The supercurrent flowing from one electrode

to the other through the nanowire is proportional to the difference of the phases of the condensate wave functions in each of the electrodes. If the wave function in the wire is coherent, the phase difference remains unchanged (provided also that no voltage difference is applied) and the supercurrent remains unchanged over time. Thus, the resistance of the wire is exactly zero if quantum coherence is unbroken. On the other hand, if the rate of occurrence of decoherence events (i.e. Little's phase slips[26]) is not zero, a proportional voltage occurs between the electrodes. Thus, by measuring the voltage (with a weak constant current being applied through the wire) we determine the rate at which the phase-coherence-breaking phase slips occur. We find that at low bias-current this rate of phase slips follows the Arrhenius thermal-activation law. Similar results have recently been obtained in experiments on thin wires fabricated from high-temperature superconductor materials.[27] No signatures of quantum tunneling of the phase slips was observed in our short wires at *low bias-currents*. However, at high bias-currents, i.e. at currents close to the critical current of the nanowire, we do observe a clear signature of quantum phase slips (QPS), viz. strong fluctuations in the currents at which switching to a resistive state occurs.[28]

Double-wire devices consist of two thin-film electrodes, connected electrically to one another through a pair of parallel superconducting nanowires.[21] Such devices have enabled us to observe a novel quantum interference effect in a magnetic field. Well-known examples of quantum interference include critical-current oscillations in conventional superconducting quantum interference devices (known as SQUIDs)[29,30] and Little- Parks resistance oscillations in thin-walled cylinders.[31] In these examples, the periods of the oscillations are controlled by the superconducting flux quantum $\Phi_0(\equiv h/2e)$ divided by the geometrical area enclosing the

magnetic field. (Here, h is Planck's constant and $-e$ is the electronic charge.) Our results on two-wire interferometers can not be explained by the Little-Parks effect, which involves oscillations of the critical temperature. We have provided a quantitative theoretical explanation for the observed period and amplitude of the oscillations, by considering the gradients in the phase of the superconducting order in the leads, which are generated consistent with the flow of Meissner screening currents. Based on this understanding, we constructed a device that is sensitive to the superconducting wavefunction phase gradients and have thus been able to measure phase differences.[22]

2 Fabricating Nanowires Using Molecular Templates

The technique of molecular templating (MT)[15] can be used to fabricate homogeneous metallic wires having ultrasmall dimensions, i.e., of diameters significantly less than $\sim 10\,\mathrm{nm}$ and lengths as small as $\sim 30\,\mathrm{nm}$. One important advantage of MT is that, as produced, the nanowires are seamlessly connected to metallic electrodes, thus making them ideal for transport measurements of various types. Another advantage is that the technique can be generalized to various materials and also to a range of geometries, if substrate molecules (or molecular assemblies) of the desired geometry can be synthesized and obtained in a suspended state.

In the MT method (see Figure 1), fabrication starts with an Si (100) wafer covered with a $500\,\mathrm{nm}$ thick layer of SiO_2 (including a $100\,\mathrm{nm}$ thick film of "dry oxide" and a $400\,\mathrm{nm}$ thick film of "wet oxide") and a $60\,\mathrm{nm}$ thick film of low stress SiN deposited by LPCVD (low pressure chemical vapor deposition) over the oxide layer.[32] In the next fabrication step, a narrow ($\sim 100\,\mathrm{nm}$) and long

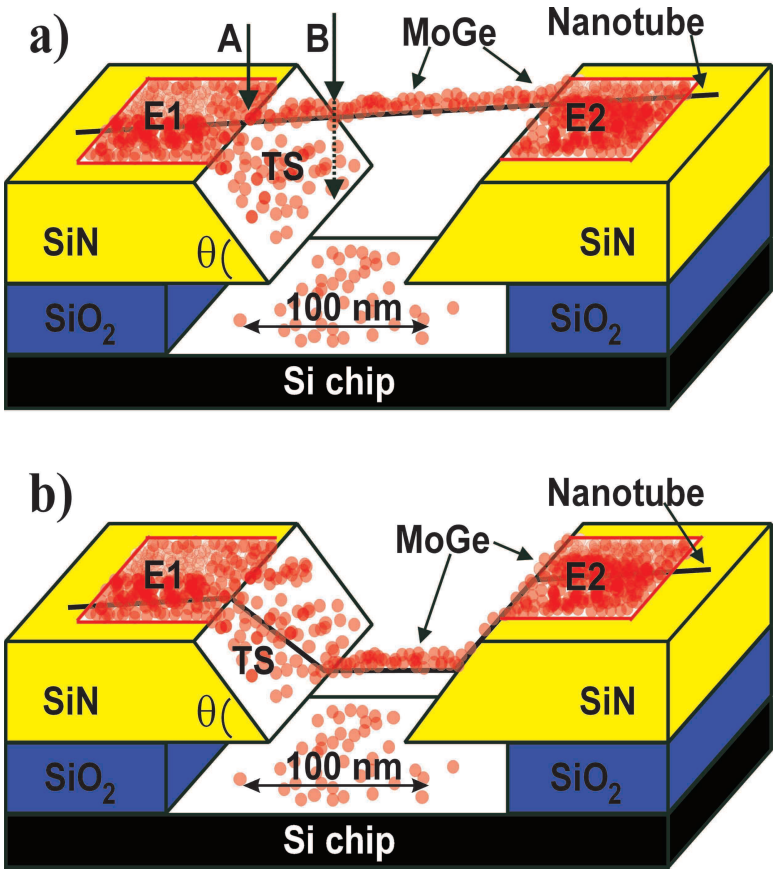

Figure 1: Schematic explanation of the principle of molecular templating (drawing not to scale).[20] (a) MT method in the ideal case, with the molecule remaining perfectly straight. A nanotube is positioned over a narrow ($\sim 100\,\mathrm{nm}$) trench etched into the top SiN layer (yellow). The film of SiO_2 positioned directly under the SiN film is used to create an undercut via HF wet etching. In order to make the the sample out of a metallic nanowire, the desired metal—typically $Mo_{79}Ge_{21}$ or Nb—is sputter-deposited over the entire surface of the Si chip, including the molecule suspended over the trench. As the sputtered metal atoms (red circles) stick to the suspended nanotube, a metallic nanowire forms on the surface of the nanotube. The electrodes, which are thin MoGe films, usually $\sim 15\,\mu\mathrm{m}$ wide, are marked E1 and E2. In a real sample, the electrode smoothly transition into larger-area contact pads, with at least two pads on each side of the trench. The contact pads are not shown here. The segment of the wire located between arrows A and B is suspended over the tilted sides (TS) of the trench, and therefore it appears as a "white spot" when imaged using a scanning electron microscope (SEM). (b) A similar sample, but with the molecule bending down into the trench. Such samples do not show "white spots" in SEM images. Such an arrangement is typical for molecules, such as DNA, which are flexible on the lengthscale of the trench width, as they tend to adhere to surfaces and thus "prefer" to cross the trench at points where the gap is the narrowest.

($\sim 5\,\mathrm{mm}$) trench is defined in the top layer of SiN using electron beam (e-beam) lithography with PMMA resist, followed by reactive ion etching using SF_6 plasma. A focused ion beam (FIB) can be used instead of electron-beam lithography to form the trench. An undercut (see Figure 1) surrounding the trench is then formed by wet etching in 50% HF for $\sim 10\,\mathrm{s}$. A less concentrated HF solution can also be used, but the etching time should then be increased. The undercut develops because the etching rate of the oxide is much larger than the etching rate of the nitride. We typically try to make the undercut to be about $300\,\mathrm{nm}$ in width, on each side of the trench. The undercut is very important for proper device operation, as it ensures that the electrodes formed in the subsequent metal sputtering step are electrically disconnected everywhere except through the nanowire. The deposition of molecules is done from the liquid phase, which can be a solution of fluorinated nanotubes in isopropanol or a suspension of regular nanotubes in dichloroethane, or a water solution containing $\lambda-$DNA molecules. The solvent can either be removed by blowing dry nitrogen gas over the sample or, in the case of DNA deposition, by placing the sample into a desiccator and pumping it out.

After the solvent is dried out, a metallic film is sputter-deposited over the entire sample. For each sample only one sputtering run is made, in which the wire and the leads are produced simultaneously. The sputtering system used was AJA ATC 2000 with the base pressure below $\sim 10^{-7}\,\mathrm{Torr}$. To keep films free of contaminants, the sputtering rate should not be too low; typically it was $\sim 0.13\,\mathrm{nm/s}$. The sputterer is equipped with a liquid nitrogen cold trap that is essential for reducing oxygen and organic impurities in the sputtered films. Contamination entering MoGe films during the sputtering can heavily suppress their superconducting properties, and thus should be avoided by all means.

After the sputtering, each molecule suspended over the trench has become coated with metal, and thus is transformed into a very thin metallic nanowire. The distribution of metal around the molecule is not know, but usually it is not important, as the diameter of the wire is smaller than or about equal to the coherence length of the superconducting material used. Preliminary tests involving transmission electron microscope (TEM) imaging of wires at various angles suggest that most of the deposited metal sits on top of the nanotube, i.e., the molecule is not located in the center of the formed wire but, rather, it lies close to the bottom of the wire.

After the sputter-deposition step, the Si chip is examined under a scanning electron microscope (SEM) and a wire without any visible defects is selected. Under "visible defects" we understand interruption and/or constrictions, or other imperfections, which can be seen on scanning electron microscope (SEM) images of the examined nanowire.

After a solitary and defect-free wire is found, its position is determined with respect to a periodic set of markers located near and along the trench. Then, the sample is spin-coated with a photoresist and subjected to photolithography, while the optical mask alignment is guided by the markers. The markers, which are simply numbers etched into the SiN film, have typical dimensions of about 5 to $10\,\mu\mathrm{m}$, so they are clearly visible in the optical microscope used to align the photomask. The markers are spaced periodically along the trench with a step of $\sim 20\,\mu\mathrm{m}$. Making samples with just one wire connecting the electrodes is possible because the concentration of wires can be made sufficiently low, typically one per every $\sim 100\,\mu\mathrm{m}$ of the trench length, while the width of the electrodes, defined by the photomask, is usually five to ten times smaller than this.

The purpose of photolithogrpahy is to protect the selected wire and, at the same time, to define the electrodes and the contact pads. After the photoresist is exposed and developed, the sample is etched either in hydrogen peroxide (for MoGe) or in a reactive ion etching (RIE) chamber (for Nb wires). As a result a sample is obtained that now has contact pads connected to $\sim 15\,\mu\mathrm{m}$ wide electrodes, which approach the trench from opposite sides, the wire serving as a weak electrical link bridging the trench and connecting the electrodes to one other. After the electrodes are patterned, the sample is examined under an SEM. If the number of wires connecting the electrodes is larger than the desired number (which is usually either one or two), the undesired wires can be removed using FIB. In most cases, though, is was possible to avoid the FIB step by positioning the photomask over a segment of the trench between two markers where there were the desired number of wires (one or two).

Unlike in the simplified schematic drawing of Figure 1a, in a practical device the number of contact pads has to be at least four,[15] with two contact pads connected to each of the electrodes. Usually, the mask is designed in such manner that there are three contact pads on one side of the trench (instead of two). Having an extra electrode allows one to measure the voltage drop on the film forming the electrodes, and to determine its critical temperature.

The Si chip with the sample is installed into a plastic chip carrier with nonmagnetic metallic pins. The connection of the contact pads to the pins is done using gold wires and indium dots and/or conducting silver paste. The person making the connections must always be grounded, in order to prevent the burning of the wire with static electricity.

SEM imaging shows that MT-produced nanowires are continuous and homo-

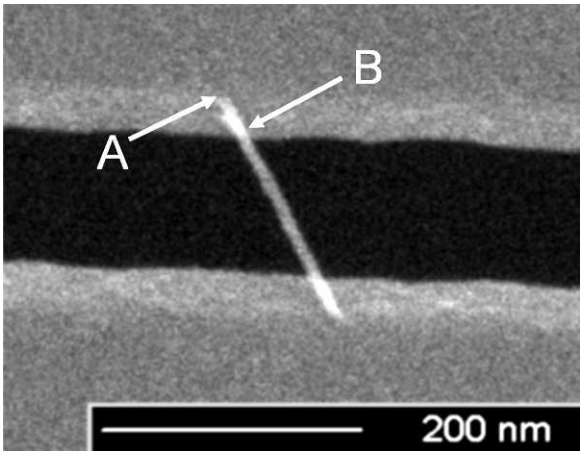

Figure 2: A scanning electron micrograph (SEM) of a MoGe nanowire (gray) suspended over a trench (black) and seamlessly connecting to two MoGe electrodes (gray areas on the top and on the bottom).[20] The white spots are visible on both sides of the wire, indicating that the wire is straight and well suspended. The beginning and end of one of the white spots are marked by arrows A and B, corresponding to the A and B arrows of Figure 1a.

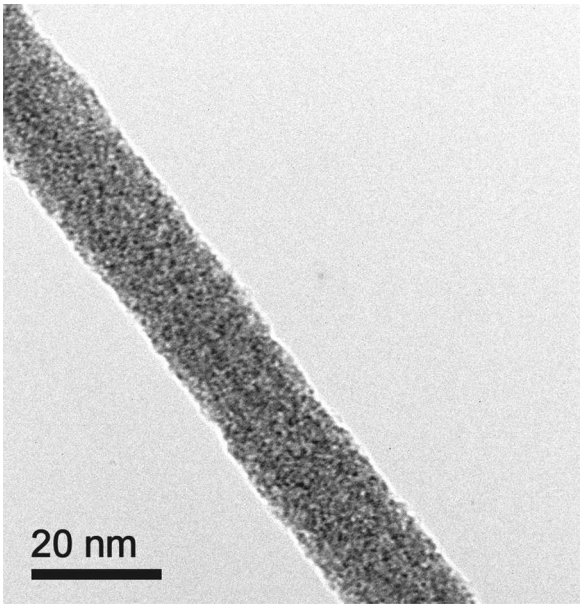

Figure 3: A transmission electron micrograph (TEM) of a nanowire templated by a fluorinated carbon nanotube. The wire appears amorphous and morphologically homogeneous, without any noticeable granularity.[33]

geneous (Figure 2). Some apparent surface roughness can be attributed to the amorphous structure of the wire (meaning a random arrangement of atoms) and to oxidation of its surface, as the nanowires are exposed to air during the fabrication steps. Imaging under a transmission electron microscope (TEM) confirms that the wires are structurally homogeneous and amorphous (see Figure 3).

2.1 Choice of Templating Molecules

The molecule used as a suspended substrate or template must be rigid enough, stable and straight. The molecule must not break when the solvent evaporates. It has to remain straight after the sample is dried and the molecule becomes suspended by its ends. The sputter-deposition process used to coat the molecule with metal is a room-temperature procedure, which is mild enough that organic molecules such as DNA can withstand the process and maintain their structural integrity during the deposition. It was found empirically that an amorphous molybdenum-germanium (MoGe) alloy has good adhesion to DNA molecules as well as to single-wall carbon nanotubes.[15,21] To date, the MT technique has been successfully used with various types of molecules, including carbon nanotubes,[15,17,34] fluorinated carbon nanotubes (fluorotubes),[35,36] DNA molecules,[21,22] as well as with nanorods.[37,38]

When using carbon nanotubes as templates in our experiments, we chose fluorinated carbon nanotubes because these molecules, unlike regular nanotubes, are perfectly insulating, because the π-electrons on their surfaces are passivated with fluorine atoms.[36] Thus, fluorotubes provide ideal templates for experiments in which the templating molecules have to be insulating. Theoretical modeling of such devices is easier, because all applied electrical current flows through the metallic coating of the molecule.

2.2 Details of the Deposition Process for DNA Molecules

We begin with a solution of λ-DNA in water, with concentration $\sim 500\,\mu\mathrm{g/ml}$, purchased from Promega. Although shorter-length of DNA could cross the $\sim 100\,\mathrm{nm}$ gap, λ-DNA, which is $\sim 16\,\mu\mathrm{m}$ long, is readily accessible and was used in all reported experiments. The stock solution of λ-DNA is very concentrated, and must be diluted for the purpose of deposition over the trench, in order to ensure that the average distance between molecules is many microns. Through multiple trials,[39] it was found that diluting the stock solution (through a serial dilution with pure DI water) to concentrations of 2 to $5\,\mu\,\mathrm{g/ml}$ works well for producing areas along the trench where only one or two molecules cross the gap every $\sim 20\,\mu\mathrm{m}$ along the trench. The width of the electrodes defined by the photomask was $\sim 15\,\mu\mathrm{m}$, so if the distance between molecules is more than that, it is always possible to address one molecule. With this mask, for the purpose of making a sample having two wires, one needs to find two wires crossing the trench, such that the distance between the selected two wires is less than $15\,\mu\mathrm{m}$, whilst the distance to other wires is larger than 10 to $20\,\mu\mathrm{m}$. Whenever we transfer a solution containing DNA through a micro-pipette, it is recommended that one widen the pipette output to $\sim 1\,\mathrm{mm}$ in diameter, to ensure the easy passage of long DNA molecules. After the solution of DNA has been diluted, a $4\,\mu\mathrm{l}$ drop is placed on the surface of the Si chip containing the trench. The chip is then placed in a dessicator to dry under vacuum. As the stock solution contains some buffer salts, which dry as crystals on the surface, it is necessary to rinse the chip in DI water after the DNA deposition. The λ-DNA molecules become heavily fixed to the surface upon drying, due to van der Waals forces, and they do not wash away in DI water.

The end result is that some of the DNA molecules dry crossing the trench. An important fact is that the molecules crossing the trench are pulled straight during the drying process, and always dry nearly perpendicular to the trench. Probably, owing to the van der Waals attraction, the DNA has a lower energy per unit length when it is bound to the SiN membrane, compared to the suspended molecule. Thus, the length of the suspended segment is minimized, leading to the result that all suspended molecule are straight and roughly perpendicular to the trench sides. After the sample is dried completely, it is ready for metal deposition. A thin metallic film is deposited over DNA molecules, thus converting them into thin wires suspended across the trench.

2.3 Significance of "White Spots"

What we call "white spots" are the short, bright, regions visible on SEM micrographs at the ends of many but not all of the nanowires. White spots occur near the points where the wire connects to the electrodes (see Figure 2). As we shall explain in detail, below, the occurrence of such white spots on SEM micrographs indicates that the wire is straight and coplanar with the leads. Thus, whenever possible, they should be used as guidance in the wire selection process.

Amongst the many wires formed across the trench after the sputtering process, it is necessary to select one that makes good electrical connection to the electrodes and which is, preferably, straight and coplanar with the electrodes. It turns our that in some cases the wire might not be coplanar if the templating molecule remains on the surface down the entire tilted side, and crosses the trench somewhere at the level of the bottom surface of the SiN film, as illustrated in Figure 1b. In such cases, the film electrodes would not be not connected to the wire directly,

but through the tilted regions on the inner sides of the trench, marked as "TS" in Figure 1. (TS stands for tilted sides of the trench.)

A typical width for the TS region is $\sim 100\,\mathrm{nm}$. The tilted sides of the trench might not be as well metallized as the top surface of the SiN film. Therefore, the TS regions can exhibit suppressed superconducting characteristics, unless the nominal thickness of the sputtered superconducting film is large enough to cover the TS regions well enough. Thus, it is important to know which of the two configurations, shown schematically as Figure 1a or 1b, is realized in any given device. A way to distinguish between these configurations is to examine SEM micrographs of the wire and check for white spots. White spots do occur if the molecule is straight (see Figures 2 and 1a), and do not occur if the molecule is bending down into the trench and crossing the gap at the level of the bottom surface of the SiN film (see Figures 4b and 1b). It is observed that carbon nanotubes are more robust and show white spots in most cases, unless the trench on which the molecule is placed is very wide, i.e., much wider than $\sim 300\,\mathrm{nm}$. DNA molecules, on the other hand, are flexible, so they almost never show white spots (see Figure 4a), even if the trench is as narrow as $100\,\mathrm{nm}$ or less. This indicates that the molecule crosses the trench at the bottom surface of the SiN membrane. This fact was directly confirmed via the imaging of tilted samples, which shows that the suspended DNA molecule cross the trench near its bottom (see Figure 4a), probably because the width of the trench is slightly smaller there. So, when DNA molecules are used as templates it is necessary to sputter thicker superconducting films, in order to ensure that the TS regions, which are measured in series with the wire, do not reduce superconducting characteristics, such as the critical temperature and the critical current of the device. Typically, we had to sputter at least $9\,\mathrm{nm}$ MoGe films in

double-wire devices that were templated by DNA, in order to make samples fully superconducting.[21] As the metal deposition process used here is sputtering, which is not a directional process, coating of the tilted sides with metal is not impossible, but simply requires a longer deposition time in order to allow the sputtered metal to coat well the TS region. White spots do not occur when the wires are long, even if carbon nanotubes are used as the template. For example, if the trench is $\sim 500\,\mathrm{nm}$ wide, white spots usually are not observed. Thus, if the metallic films are not thick enough, such long samples frequently show multiple resistive transitions, due to the involvement of weakly superconducting TS regions. This issue becomes critical in cases in which the films must be thin, e.g., in studies of the superconductor-insulator transition (SIT).[16] Such studies can only be done on relatively short samples, and only with nanotubes acting as templates. The trench must be narrow because if it were wider than $\sim 300\,\mathrm{nm}$ then the deposited nanotubes would frequently curve themselves into the trench.[16]

Now we explain why such white spots occur. The beginning and end of one such white region are indicated by the arrows marked 'A' and 'B' in Figure 2. The reason for the appearance of these bright regions at the ends of the wire is that the segment of wire between points A and B is suspended over a tilted side of a trench, and this tilted side is also covered by metal, as illustrated in Figure 1a. In fact, as the sputtering is a more or less isotropic deposition process, the TS becomes metallized even underneath the wire. Thus, the micrograph contains superimposed images of both the wire and the side of the trench right under it. Together, the wire and the TS scatter more electrons, and thus make the ends of the wire brighter than the central part of the wire positioned over the empty space of the trench. Figure 1 shows that white spots can only occur if the width of the trench is narrower at its

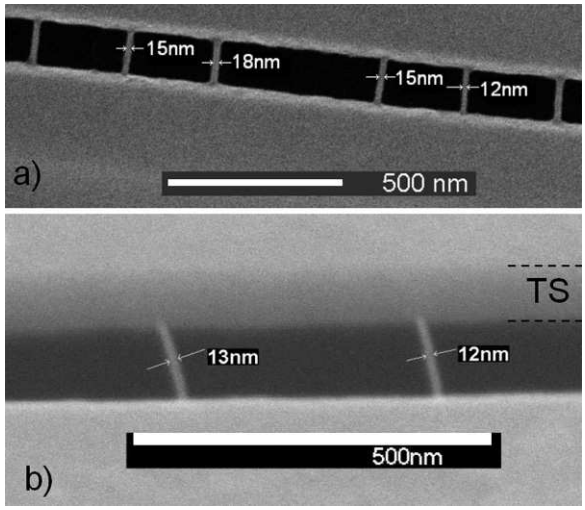

Figure 4: SEM micrograph of nanowires made using DNA templates. The wires appear morphologically homogeneous, without noticeable granularity. The apparent width of the wires are indicated on each image. The actual width of the metallic core is thinner than the indicated number, e.g., due to surface oxidation (usually by $5\,\mathrm{nm}$), carbon coating of the wires during SEM imaging, or SEM resolution limitations. (a) Top view of a sample with a trench (black) crossed by six nanowires templated using DNA molecules. (b) SEM image of a tilted sample, which shows that DNA crosses the trench at the trench bottom. The two horizontal dashed lines with letters TS show the width of the membrane, which is called the "tilted side" in the text.[39]

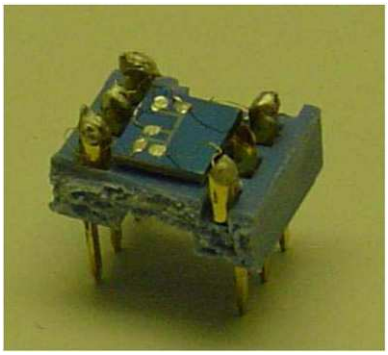

Figure 5: A photograph of the chip carrier having a mounted Si chip. Either four or five of the six pins are typically connected to the sample by gold wires and indium dots. The MoGe electrode pattern with the five pads can be seen in the image. The chip itself is $4.8\,\mathrm{mm}$ by $4.8\,\mathrm{mm}$. Due to small dimensions the wire and the trench are not visible in this image.[39]

bottom than at its top. Exactly this situation occurs, due to the isotropic nature of the SF_6 reactive ion etching (RIE), which is typically employed to etch the trench into the SiN film.

3 Preparing the Sample for Measurements

After the fabrication process is finished, the sample is mounted for electrical measurements. The mounting procedure is very dangerous for the wires, as this is when many of them are typically burned by unwanted static electricity.

To ensure the successful mounting of the wire, the person making the mounting should be electrically grounded, e.g., with an anti-static wristband and a seat that is sprayed with an anti-static solution. We mount the Si chip on to a plastic chip carrier with six metallic pins, (Figure 5) which are either nonmagnetic or only slightly magnetic due to their Ni plating. Electrical connections between the pins of the chip carrier and the contact pads on the Si chip are made using $50\,\mu\mathrm{m}$ diameter gold wire. First, four or five gold wires, each $\sim 1\,\mathrm{cm}$ long, are soldered

(or attached using silver paint) to desired pins of the chip carrier. Then, a small piece of double-sided sticky carbon tape (which is typically used for mounting samples in SEM) is placed in the center of the chip carrier, and the sample is placed over the carbon tape. The tape serves the purpose of fixing the sample on the surface of the chip carrier. One needs to make sure that the tape does not touch any of the pins of the chip carrier. Next, the free ends of the gold wires are connected to the corresponding contact pad of the sample using $\sim 250\,\mu\mathrm{m}$ diameter indium spheres. This is done as follows. One sphere is placed on the contact pad and pressed from the top with the flat-backed surface of a stainless steel drill bit (or with the end of a metal lead of a common commercial resistor). Then, the corresponding gold wire is placed over the In dot and pressed again. Finally, another In dot is placed over the gold wire and pressed one more time. The second In dot is needed in order to reduce electrical resistance of the contact and make the connection reliable enough that it can withstand the process of cooling the sample down to cryogenic temperatures. With some training, such a connection process allows one to connect thin gold wires to a thin-film MoGe contact pad of the sample without using a soldering iron or ultrasonic bonder (either of which might bring an unwanted voltage to the sample and thus burn the wire). Once all the pads have been connected to the pins of the chip carrier, the chip carrier is inserted into a matching socket positioned on one "cold finger" of the cryostat. In most cases Janis ^{3}He cryostat (from Janis Research), which reaches down to a temperature of $0.28\,\mathrm{K}$, was used for the measurments. The sample is cooled exclusively through the measurement leads. The leads, made of a resistive thin wire (e.g., $50\,\mu\mathrm{m}$ nylon-coated nickelchrome alloy wires, Stablohm 800A,' California Fine Wire Co., Grover Beach, CA, USA) are wound (at least ten times) around the cold

finger, and coated with a thick layer of dense silver paste and/or a layer of epoxy with mixed-in Cu particles. The coating glue allows a good thermal connection of the leads to the cold finger of the cryostat and thus allows the leads to be cooled to the base temperature. The coating of the leads with a glue containing metallic particles cuts down electromagnetic noise (i.e., black-body radiation from the top of the cryostat).[40] It is advantageous to select leads made of thin resistive wires, as in this case they bring less heat and less electromagnetic noise loads to the sample. The leads are connected to the metallic pins of a plastic socket, into which the chip carrier is inserted. Thus, the pins of the chip carrier are cooled through the connection to the leads. The pins of the chip carrier are connected through the gold wires to the sample, ensuring the cooling of the sample's contact pads and, through them, the entire sample, including the nanowire. The thermometer, a calibrated RuO (or Cernox) resistor purchased from LakeShore Cryotronics Inc., is mounted in the same way as the sample, on a separate chip carrier. Thus, the thermometer is also cooled to the base temperature through the leads, which are thermalized in the same way as the wires leading to the sample. The sample and thermometer chip carriers are placed into the same socket, which has a sufficient number of leads and which was placed inside a brass-made, full-metal Faraday cage.

4 Electrical Transport Measurements

The sample is biased with an AC current at a frequency of $\sim 11\,\mathrm{Hz}$ and amplitude in the range 1 to $10\,\mathrm{nA}$. The current bias is achieved by using an ultralow-distortion function generator (Stanford Research Systems DS 360). The voltage from the

generator is applied to the sample through a standard resistor having a value of $\sim 1\,\mathrm{M}\Omega$, which is much larger than the typical resistance of the sample and the leads connected to the sample (which is ~ 1 to $10\,\mathrm{k}\Omega$). Thus, the current through the sample, connected in series with the standard resistor, is mostly determined by the value of the resistor. This current is recorded, as a function of time, by measuring the voltage across the standard resistor and dividing the measured voltage by the resistance of the resistor. The voltage on the superconducting electrodes is also measured (with a separate pair of leads) and recoded, as a function of time. Both measurements are done using battery-powered preamps (either Princeton Applied Research model 113 or Stanford Research Systems model SR 560). After one period of the sinusoidally time-dependent bias current is completed, the recorded voltage V is plotted as a function of current I. Thus, the $V(I)$ curve is obtained, and is plotted on the screen of a computer using LabVIEW software. In order to determine the linear resistance of the sample (also called zero-bias resistance), the current-bias amplitude is chosen to be small enough that the $V(I)$ curve is linear. Then, the best linear fit to the $V(I)$ curve is found using LabVIEW functions. The slope of the linear fit is defined to be the resistance R of the sample.

At low enough temperatures ($\lesssim 1\,\mathrm{K}$), typical nanowires, if they are not too thin, show pronounced signs of superconductivity. The wire has to be "not too thin" because wires that are thinner than some length- and material-dependent critical diameter do not exhibit any signs of superconductivity, but, rather, can be characterized as slightly insulating.[16] Most notably, the resistance R of the sample becomes immeasurably small at low temperatures. For the type of measurement outlined above, the lowest value of R that can be measured is roughly $1\,\Omega$. This

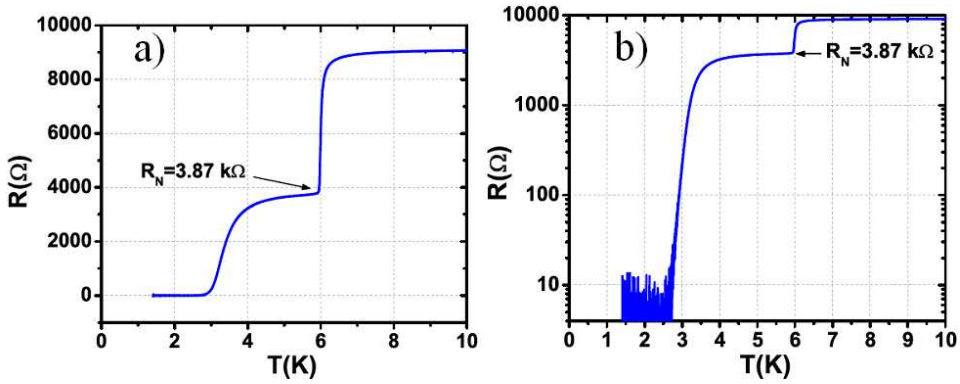

Figure 6: $R(T)$ curve for a typical sample involving a single MoGe nanowire.[41] The template used to make the wire was a fluorinated carbon nanotube. (a) Sample resistance is plotted versus temperature in a linear format. The first resistive transition, occurring at $\sim 6.0\,\mathrm{K}$, is due to the superconducting transition taking place in the film electrodes that lead to the wire. The second apparent transition, at $\sim 3.5\,\mathrm{K}$, corresponds to the occurrence of superconducting behavior in the nanowire. (b) The same data as in (a), plotted in a log-linear format. The negative curvature of the bottom part of the curve indicates that the wire resistance drops, with cooling, at a rate that is faster than exponential.

lowest value is called the "noise floor" of the setup. As the temperature of the sample is reduced below a certain value, R drops below the noise floor and cannot be measured. At such low temperatures, we perform a complementary measurement, viz., a measurement of the switching current I_{SW}. To do this, the bias current is slowly increased until a sharp, jump-wise increase in R is observed. In such jumps, R increases from apparently zero up to the normal resistance of the wire R_{N}. The current at which the jump occurs is called I_{SW}. After the switching event, the wire goes into the normal state, due to excessive Joule heating. To return the wire to the superconducting state, one needs to reduce the bias current considerably. The current at which the wire switches back to the superconducting regime is called the "retrapping current" I_{R}.

A typical dependence of the sample resistance on temperature $R(T)$ is shown

in Figure 6a. Figure 6b shows the same data plotted in the log-linear format. Due to the fact that the wire is connected in series with the thin film electrodes, two resistive transitions are observed. To explain the occurrence of the two transitions, we note that the voltage leads are not connected to the wire itself (because the wire is very short) but to the electrodes connected to the wire. If the electrodes are in the normal state, the bias current flowing through the electrodes causes extra voltage, and the measured resistance becomes larger than the normal resistance of the wire. On the other hand, at $\sim 6\,\mathrm{K}$ the electrodes E1 and E2 (see Figure 6) become superconducting. Thus, below this temperature the measured resistance is entirely due to the nanowire. Such a conclusion was confirmed by independent measurements on thin film electrodes.[15] The second transition (at $\sim 3.5\,\mathrm{K}$) is due to the nanowire losing its resistance. In all measured samples it was found that wires made of MoGe alloy show a lower critical temperature, compared to films of the same thickness. This reduction of the critical temperature may be due to reduction of the screening of the Coulomb repulsion between the electrons.[42] We define the normal-state resistance of the wire R_{N} to be the sample resistance measured immediately below the temperature at which the leads become superconducting, as shown by the arrows in Figure 6.

Voltage-current characteristics, measured at various temperatures, of a typical sample with a single nanowire are shown in Figure 7. The larger arrows show the directions of sweeping of the bias current. The switching current I_{SW} is marked by the upward arrow. When the bias current is increased to the value of I_{SW} the wire switches abruptly to a resistive state, which is, in fact, the normal state of the wire, maintained by Joule heating.[43] The retrapping current I_{R} is marked by the downward arrow. The transition at I_{R} is also abrupt. It is clear from the graph

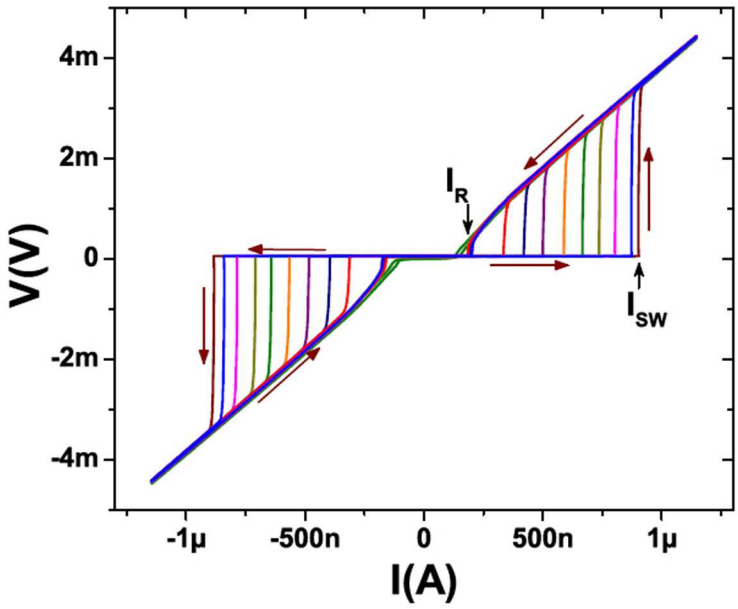

Figure 7: A series of voltage versus current curves $V(I)$ of a typical sample involving a single MoGe nanowire, measured at various temperatures.[41] The switching current I_{SW} and the retrapping current I_{R} are indicated for the curve measured at $0.28\,\mathrm{K}$. The corresponding temperatures are $0.28\,\mathrm{K}$ (corresponding to the highest I_{SW}), $0.4\,\mathrm{K}$, $0.6\,\mathrm{K}$, $0.8\,\mathrm{K}$, $1.0\,\mathrm{K}$, $1.2\,\mathrm{K}$, $1.4\,\mathrm{K}$, $1.6\,\mathrm{K}$, $1.8\,\mathrm{K}$, $2.34\,\mathrm{K}$. In all cases it is found that as the temperature is increased the value of I_{SW} decreases. This sample was made using a fluorinated carbon nanotube as template molecule.

that the switching current is very sensitive to changes in temperature. As the temperature is increased, the $I_{\rm SW}$ decreases significantly. On the contrary, the $I_{\rm R}$ is almost independent of temperature, until the temperature reaches a high value of $T \sim 2\,{\rm K}$, at which a noticeable decrease in $I_{\rm R}$ is found with increasing the temperature.

5 Little's Phase Slip as a Mechanism of Supercurrent Dissipation

Consider a model: a thin superconducting wire forming a closed loop.[26] Suppose the initial state of the system is such that the supercurrent $I_{\rm S}$ in the loop is such that $0 < I_S < I_{\rm C}$, where $I_{\rm C}$ is the critical current of the wire, i.e., the current that is sufficient to destroy superconductivity. If fluctuations are weak, such a state of the system would persist indefinitely. The analysis by Little[26] shows that only strong fluctuations, viz., those that bring the order parameter to zero at some spot along the wire, can cause the supercurrent to decay.

The reason is the following. In a superconducting wire, $I_{\rm S} \sim \phi/L$, where L is the wire length (or the loop length) and ϕ is the difference in the phase of the complex-valued wavefunction describing the superconducting condensate. The phase difference is taken between the ends of the wire, if the wire is connected to superconducting electrodes. In Little's model, the wire forms a loop, and so ϕ stands for the phase accumulated along the closed path coinciding with the the loop itself. As the wavefunction must be single-valued, the phase difference around a closed loop is always $\phi = 2\pi n$. Here, n is an integer, which sometimes is called the "vorticity" of the state and can be regarded as the number of core-less vortices trapped within the loop. (NB: We are assuming here that the magnetic

field is zero everywhere.) The fact is that unless n is changed the current $I_{\rm S}$ cannot change, because $I_{\rm S} = const \times \phi = {\rm const.} \times n$. Little's topological analysis of the loop model shows that the phase difference ϕ can only change if a strong and rare fluctuation occurs, such that it brings the amplitude of the complex wavefunction describing the condensate (sometimes called superconducting "order parameter") to zero at some point on the wire. If this happens, the phase can change by 2π (or integer multiples of it.) One way to understand this is to realize that without a magnetic field the supercurrent in the loop is proportional to the number of core-less vortices n trapped within the loop. To reduce the value of the supercurrent a vortex must be expelled from the loop. To exit the loop, the core of a vortex must cross the loop at some point. Thus, there is an energy barrier for such process, which is roughly equal to the energy of the vortex core positioned somewhere on the wire that forms the loop. The vortex core is simply a normal (i.e., non-superconducting) region of size roughly the superconducting coherence length $\xi(T)$. At low temperatures, the free energy of the superconducting state is lower than the free energy of the normal state, and the difference is given by the so-called condensation energy density $H_c^2/8\pi$. Thus, the energy barrier for such vortex-crossing process ΔF can be estimated via $\Delta F \approx A\xi H_c^2/8\pi$, where $A\xi$ is the volume of the normal region associated with the normal core position on the wire, the cross-sectional area of which is A. The event when a vortex trapped in the the loop crosses the wire (that makes the loop) and escapes to infinity is an example of the so-called Little phase slip (LPS). The LPS event is illustrated in Figure 8, from which it is clear that (a) LPS can only occur if the order parameter (represented by the radius of the order-parameter spiral) reaches zero (at least instantaneously), and (b) LPS cause a change of the phase-difference by 2π, which precisely means

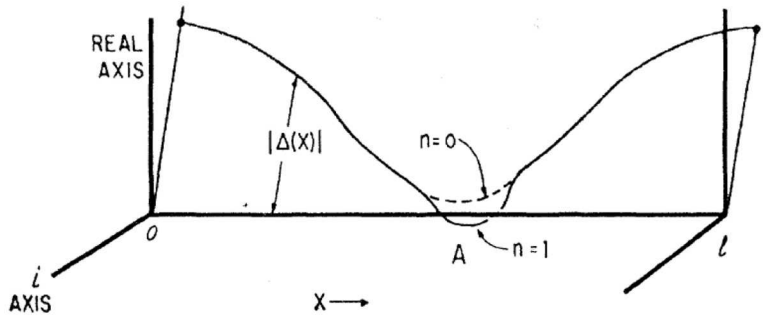

Figure 8: The original Little phase-slip diagram.[26] The complex superconducting order parameter of a thin wire loop is drawn as a function of position along the loop. "REAL AXIS" and "i AXIS" represent the real and imaginary components of the superconducting order parameter $\psi(x) = |\Delta(x)| \exp(i\phi(x))$. Two possible configurations are shown, one for an order parameter in the sub-ensemble $n = 0$ (i.e., no vortices trapped in the loop), and the other one is for $n = 1$ (i.e., one vortex present in the loop). Near the point A, $\psi_1(x)$ makes an excursion around the origin of the Argand diagram, whilst $\psi_0(x)$ does not. The transition from the $n = 1$ state to the $n = 0$ state constitutes a phase-slip event. This transition can be viewed as vortex escape, when the normal core of the vortex crosses the wire. Hence, the transition between the $n = 1$ and the $n = 0$ states can only occur if the thermal fluctuation is strong and the order parameter reaches zero somewhere along the wire, if only for a short period of time. Reaching zero is a necessary condition, because the normal core of a vortex has zero order-parameter amplitude at its center.

that the spiral, representing the order parameter in the Argand diagram, loses one turn.

The rate of thermally activated phase slips (TAPS), Γ_{TAPS}, is governed by the Arrhenius activation law and can be written as $\Gamma_{TAPS} = \Omega \exp(-\Delta F/k_B T)$. Here, Ω is an effective attempt frequency, which was estimated rigorously only for temperatures near the critical temperature.[44] At low temperatures, when thermal fluctuations are weak and the associated rate of phase slips is low, quantum fluctuations might play a role and allow the vortices trapped in a loop to escape by tunneling. Thus the supercurrent would decay due to quantum phase slip

(QPS). The rate of QPS is determined by the quantum action of the vortex core crossing the wire and can be roughly estimated, following Giordano model,[45] as $\Gamma_{QPS} = \Omega_{QPS} \exp(-\Delta F/k_B T_Q)$, where Ω_{QPS} represent some effective attempt frequency of the quantum fluctuations of the order parameter amplitude and T_Q is a phenomenological parameter (quantum temperature) defining the strength of quantum fluctuations.

One of the goals of developing the theory of phase slips is to be able to predict the temperature dependence of the resistance of a thin wire, $R(T)$, such as those shown in Figure 6. The main hypothesis needed for the calculation is that even if the wire is not forming the loop but, instead, it is connected to some external leads, which are used to inject the current into the wire, the resistance of the wire would be determined exclusively by the LPS rate (assuming that a dc measurement is considered). A detailed theoretical analysis of such situation was given by Langer and Ambegaokar[46] and by McCumber and Halperin.[44] The corresponding theory is called LAMH theory. This theory does not take into account the possibility of QPS but only treats TAPS.

Here, we list the corresponding formulas. Within the LAMH theory the resistance is predicted to be $R_{\rm LAMH}(T) = R_{\rm Q}(\hbar\Omega_{TAPS}/k_{\rm B}T)\exp(-\Delta F(T)/k_{\rm B}T)$, where $\hbar = h/2\pi$, h is Planck's constant, $k_{\rm B}$ is Boltzmann's constant, $\Delta F(T)$ is the temperature-dependent barrier for phase slips, and $R_{\rm Q} = h/4e^2 = 6.5$ kΩ is the quantum of resistance (in which $-e$ is the charge of the electron).[30] In the LAMH model, the attempt frequency is given by[44]

$$\Omega_{\rm LAMH} = \big(1/\tau_{\rm GL}\big)\big(L/\xi(T)\big)\sqrt{\Delta F(T)/k_{\rm B}T}. \qquad (1)$$

Here, $\tau_{\rm GL} = \pi\hbar/8k_B(T_C - T)$ is the so-called Ginzburg-Landau relaxation time.

LAMH theory is only valid near $T_{\rm C}$, because it is based on time-dependent Ginzburg-Landau theory, which has a narrow range of applicability. By some estimates,[47] it can only be applied in a narrow range, such as $0.90T_{\rm C} < T < 0.94T_{\rm C}$.

Thus, it is desirable to have approximations applicable at lower temperatures. These approximations rely on the Arrhenius factor alone, which is correct down to zero temperature, provided that only thermal activation—but not quantum tunneling—of LPS needs to be accounted for. (Quantum tunneling will be discussed separately, below.) An approximate formula for the wire resistance caused by TAPS is $R_{\rm AL}(T) = R_N \exp(-\Delta F/k_{\rm B}T)$. It can be referred to as the Arrhenius-Little formula (AL) for the reason that the exponential factor is the usual thermal-activation law, analogous to the Arrhenius law, and the prefactor is the normal resistance of the wire. One can argue that such prefactor is reasonable, based on the Little's hypothesis that each phase slip creates a region of size $\xi(T)$ that simply acts as normal metal and has an electrical resistance of $R_{\rm N}\xi(T)/L$. One needs to take into account the fact that each segment of the wire does not stay normal at all times but, rather, becomes normal only in the rare event that an LPS occurs on the segment under consideration.[48] It should be emphasized that $R_{\rm LAMH}$ and $R_{\rm AL}$ are qualitatively distinct, in the sense that the prefactor of $R_{\rm AL}$ includes the wire's normal resistance, whereas the prefactor of $R_{\rm LAMH}$ is independent of the normal resistance of the wire. Yet, the role played by the prefactor is negligible in all practical cases so that both formulas can be used to fit the experimental $R(T)$ curves. This fact is illustrated in Figure 9, where both types of fit are shown, and both exhibit good agreement with the data. Thus, the LAMH and AL formulas can be used interchangeably to approximate the experimental results.

To complete the list of useful formulas, one needs the expression relating the

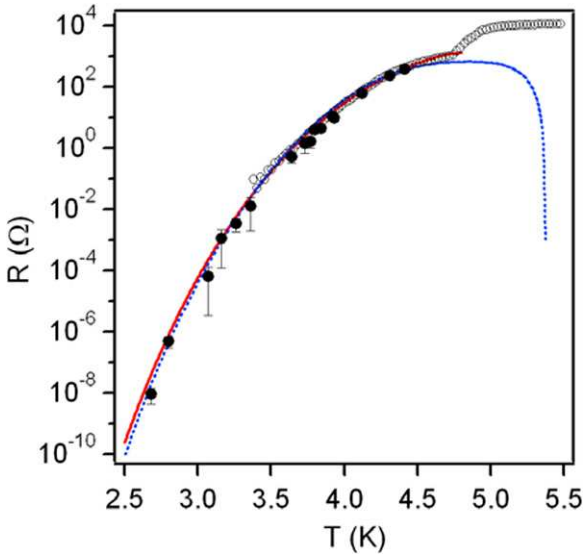

Figure 9: Resistance versus temperature for a narrow superconducting bridge, the sample B2 from Ref.[48] This samples was fabricated as is illustrated in Figure 1a, including metallization with sputtered MoGe, except that instead of a nanotube a SiN bridge was used as a template. Open circles represent direct low-bias transport measurements of the sample resistance. Filled circles represent the resistance determined indirectly, viz., by extrapolating high-bias segments of the nonlinear $V(I)$ curves. The solid (red) and the dashed (blue) curves give the best fits generated by the $R_{\rm AL}$ and $R_{\rm LAMH}$ formulas, respectively. Both models show a good agreement with the data. The downturn of the blue curve, which corresponds to LAMH theory, is an artifact of the theory that is related to the fact that the attempt frequency Ω_{LAMH} goes to zero as $T \to T_{\rm C}$.

LPS barrier $\Delta F(T)$ to the critical current of the wire $I_{\rm C}(T)$, which is[49]

$$\Delta F(T) = \sqrt{6}(\hbar/2e) I_{\rm C}(T). \tag{2}$$

Another important result is the formula

$$\Delta F(0) = 0.83 k_{\rm B} T_{\rm c}\, (R_{\rm Q}/R_{\rm N})(L/\xi(0))\,, \tag{3}$$

which relates the barrier for phase slips to the normal resistance of the wire.[49] Close to $T_{\rm C}$ the coherence length can be approximated as $\xi(T) = \xi(0)/\sqrt{1 - T/T_{\rm C}}$, where $\xi(0)$ is the zero temperature coherence length. There is also an expression for the critical current of the wire, applicable at all temperatures, viz., the Bardeen formula,[50]

$$I_{\rm C}(T) = I_{\rm C}(0)\big(1 - (T/T_{\rm C})^2\big)^{3/2}. \tag{4}$$

6 Quantum Interferometer with Two Nanowires

In this section we describe how superconducting nanowires can be used to build a quantum interferometer, which is similar but not equivalent to usual superconducting quantum interference devices (SQUIDs).[21] Our device is based on two nanowires which replace the two Josephson junctions (JJ) of a SQUID. Thus, we call our device a nanowire-SQUID or N-SQUID. The N-SQUID is presented schematically in Figure 10.

In this example, two DNA molecules are positioned across the trench, and are coated with superconducting MoGe. The magnetic field B is applied perpendicularly to the MoGe electrodes (yellow).

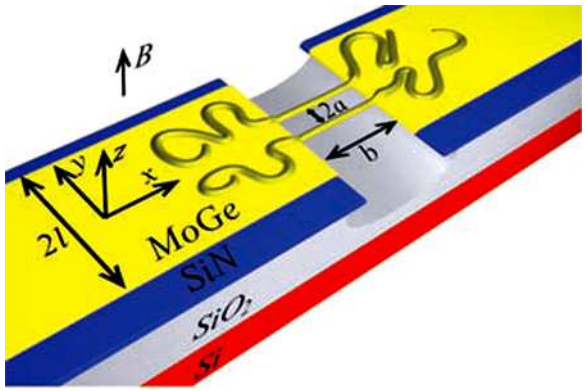

Figure 10: Schematic of a double-nanowire device, or N-SQUID, templated by two DNA molecules. Two strands of DNA are placed across a trench etched into an SiN film deposited on an oxidized Si chip. The MoGe electrodes are shown yellow. They are connected to each other via the pair of MoGe nanowires.[21,39]

6.1 Transport Measurements on an N-SQUID

Transport measurements on double-wire devices reveal a resistive transition, similar to that found in samples containing single wire. In zero magnetic field ($B = 0$), the $R(T)$ curve can be fit with the LAMH expression $R_{\mathrm{LAMH}}(T)$, as shown in Figure 11a (lower curve). As a magnetic field is applied perpendicularly to the film electrodes, the $R(T)$ curve is found to broaden and narrow periodically with the field. An example of a broadened curve is also shown in Figure 11a. It is also in agreement with the LAMH model, generalized to the case when a magnetic filed is present.[51] The generalization is made by explicitly including in the calculation the dependence of the barrier for phase slips on the superconducting wavefunction phase difference δ between the points on the electrodes at which the wires are connected. The critical current of the double-wire device can be modeled following the example of a double-Josephson-junction as[21,51]

$$I_{\mathrm{C}}(B) = \sqrt{(I_{\mathrm{C1}} + I_{\mathrm{C2}})^2 \cos^2 \delta(B) + (I_{\mathrm{C1}} - I_{\mathrm{C2}})^2 \sin^2 \delta(B)}, \qquad (5)$$

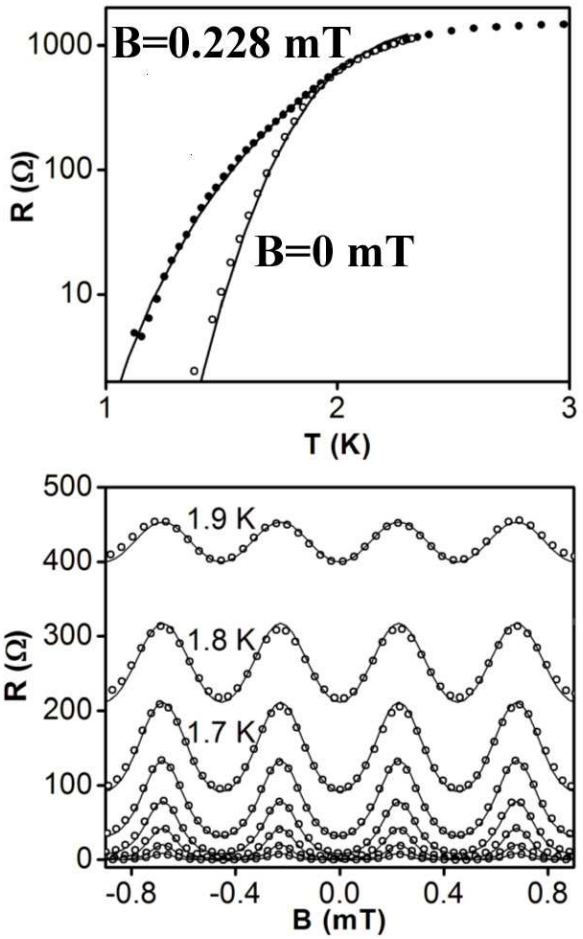

Figure 11: (a) Resistance versus temperature curves for sample "219-4," measured in zero magnetic field ($B = 0$) (open circles) and at $B = 0.228\,\mathrm{mT}$ (solid circles). The latter field corresponds to a maximum value of the resistance. This samples was fabricated as is illustrated in Figure 1a. A DNA double-helix was used as a template. The continuous curves are theoretical fits (see text) calculated with the following fitting parameters for the two wires in this sample: $I_{\mathrm{C1}}(0) = 639\,\mathrm{nA}$, $I_{\mathrm{C2}}(0) = 330\,\mathrm{nA}$, $T_{\mathrm{C1}} = 2.98\,\mathrm{K}$, and $T_{\mathrm{C2}} = 2,00\,\mathrm{K}$, with corresponding values of the coherence length $\xi_1(0) = 23\,\mathrm{nm}$ and $\xi_2(0) = 30\,\mathrm{nm}$. (b) Resistance versus magnetic field measurements on sample "219-4" at temperatures ranging from $1.2\,\mathrm{K}$ to $1.9\,\mathrm{K}$ in $0.1\,\mathrm{K}$ increments. The lines are theoretical fits computed using the same fitting parameters as in (a), with a period of the oscillation in magnetic field set to $\Delta B = 0.456\,\mathrm{mT}$.[21,39]

where the phase difference $\delta = \delta(B)$ will be discussed in detail, below. The corresponding barrier for phase slips (which defines the value of the resistance) is given by Eq. 2. The observed periodic broadening and narrowing of the resistive transition is due to the dependence of the LPS barrier on the field-dependent phase δ, as given by Eq. 5. The latter expression shows that the period of the oscillation is $\Delta\delta = \pi$. It is half of the usual period, 2π, because the two wires of the N-SQUID are connected to two electrodes, each of which imposes a phase difference δ on the pair of wires. Thus, the resulting effective phase difference, which controls the current circulating in the loop formed by the wires and the electrodes, is doubled (i.e. it is 2δ for the considered device configuration). The observed, highly pronounced, reproducible oscillations of the resistance with magnetic field (Figure 11b) are due to the periodic broadening and narrowing of the $R(T)$ curves. For higher temperatures, the resistance oscillations follow a cosine law. The period of the oscillations was found to be temperature-independent in all samples tested, in agreement with the model.[21,51]

These observations raise a question of whether there is a qualitative difference between the observed oscillations and Little-Parks oscillations, long known to occur in hollow, thin-walled, superconducting cylinders pierced with magnetic field.[31] The most notable aspect of oscillations in our double-nanowire devices is the value of the period ΔB. It turns out that ΔB is *much* smaller than one would expect on the basis of the superconducting flux quantum divided by the area of the closed loop formed by two wires and the electrodes to which they are connected (this area is $2ab$ in our notation, as shown in Figure 10). For example, for sample "219-4" we estimate the period of the Little-Parks oscillation to be $\Delta B_{\rm LP} = \phi_0/2ab \approx 25\,{\rm mT}$, with dimensions $2a = 595\,{\rm nm}$ and $b = 137\,{\rm nm}$. The

value of the period found experimentally is $\Delta B_{\rm exp} = 0.46\,{\rm mT}$. Thus, the the experiment shows a period that is more than fifty times smaller than expected. Therefore, we conclude that the observed oscillation is not controlled by the geometrical area of the closed loop defined by the nanowires and the edges of the leads. Instead, we find that in the low magnetic-field regime (i.e., when no vortices are present in the leads), the period is controlled by ϕ_0 divided by a new quantity, $4al$, which is the product of the width of the electrodes and the inter-wire spacing $2a$. Here, the width of the electrodes is denoted $2l$, and it equals $12060\,{\rm nm}$ for sample "219-4."

Our model predicts the following expression for the period of the resistance oscillation $\Delta B_{\rm theory} = (\pi^2/8G)(\phi_0/4al) \approx 0.38\,{\rm mT}$, (here, $G = 0.916...$ is the Catalan number). The prediction is close to the experimental value. Testing additional samples showed even better agreement. Namely, three additional samples were measured and the experimental values of the period were as follows: $\Delta B_{\rm exp} = 0.947; 0.077; 0.049\,{\rm mT}$. The corresponding values predicted by the theory are $\Delta B_{\rm theory} = 0.929; 0.078; 0.047\,{\rm mT}$. The agreement is excellent, except in one sample, "219-4," in which case it is just good. This single significant deviation from the predicted value is explained by the fact that one of the electrodes of sample "219-4" had a marker patterned a few micron away far from the nanowires. The presence of the marker perturbed the distribution of the supercurrent and led to a deviation of $\delta(B)$ from the model, which assumes that the electrodes are uniform. All other samples were fabricated such that markers were outside the regions occupied by superconducting electrodes. It should also be emphasized that a general assumption of the model was that $a \ll l$.

To develop the model we take into account the following facts. (1) The

leads of the double-wire device are mesoscopic—i.e., they are narrower than the perpendicular magnetic penetration depth ($\lambda_\perp \approx 70\,\mu\mathrm{m}$)—and therefore the magnetic field penetrates the leads with negligible attenuation. (2) Because the resistance is caused by thermal phase fluctuations (i.e., LPS), in very narrow wires the oscillations can be observable over a wide range of temperatures ($\sim 1\,\mathrm{K}$). (3) The Little-Parks (LP) resistance oscillation is in fact a direct consequence of the critical-temperature oscillation with magnetic field. The physics reason for the LP oscillation is that the velocity of the superconducting condensate, and therefore its free energy, are sensitive to the (continuously tunable) vector potential and on the (discrete) vorticity, which compete. The oscillation occurs as the vorticity changes to minimize the energy. The LP effect can be visualized as a rigid periodic shift of the $R(T)$ curve, with magnetic field, as the critical temperature oscillates. In contrast, in the double-wire interferometer we find a much more substantial contribution to the resistance oscillations coming from the modulation of the barrier heights for phase slips, which is manifested in a periodic broadening and narrowing of the $R(T)$ curve, and not just a shift as in the LP oscillation case. This difference (broadening versus shift) is qualitatively explained by the fact that in the device in question the oscillation is due to the effect of the magnetic field and associated vector-potential on thermal *fluctuations*, viz., on the LPS rate, whilst in the LP effect the oscillation is a mean-field effect, not related to fluctuations at all. Quite generally, the oscillation can be described as $R(T,B) = R_\mathrm{N} \exp\left(-\Delta F(T,B)/k_\mathrm{B}T\right)$. The essential ingredients in our model are (i) the leads, in which the applied magnetic field induces supercurrents and, due to this, gradients in the phase of the order parameter, and (ii) the pair of wires, whose behavior is controlled by the phase difference imposed by the leads. We

assume that the phase difference in the leads is not influenced by nanowires. The reasonableness of this assumption is justified by a very good agreement between the theory and the experiment.

6.2 Deriving the Electrode-Imposed Phase Difference Between the Wires

Now we present a simplified derivation of the dependence of the phase-difference on the magnetic field,i.e., $\delta = \delta(B)$. For a more thorough treatment of the problem, see Ref.[51] Here, we solve the problem in the coordinate system indicated in the Figure 10, with corresponding unit-length basis vectors $\hat{x}$, $\hat{y}$, and $\hat{z}$. Consider an infinitely long, thin-film, superconducting strip of width $2l$, such that $l << \lambda_{\perp}$. Assume that a uniform and perpendicular magnetic field $B\hat{z}$ is applied. The field is regarded as being sufficiently weak that no vortices are present in the strip. The vector-potential, which we take to be of the form $\vec{A} = By\hat{x}$, is always in the plane of the strip, with $\vec{A} = \vec{0}$ along the center of the strip. Thus, the two-dimensional current density, for an infinite strip, is given by $\vec{J}(x,y) = J_x\,\hat{x} = -t_f\,\vec{A}(x,y)/\mu_0\,\lambda^2 = -(t_f By/\mu_0\,\lambda^2)\hat{x}$, where t_f is the film thickness and λ is the bulk magnetic penetration depth.[30] Therefore, the magnitude of $\vec{J}$ at the edges of the electrodes that lie parallel to $\hat{x}$ is $t_f Bl/\mu_0\,\lambda^2$. In our N-SQUID device, the length of the two electrodes is much greater than their width. Thus, the above estimate for the current-density near the long edges is applicable. Nevertheless, the important fact is that our electrodes are not infinite—they end at the point where the wires start.

Due to the supercurrent conservation principle at low temperatures, the edge current flowing near one of the edges parallel to $\hat{x}$ must sweep around at the short

edges of the electrodes (i.e. the edges parallel to $\hat{y}$) and, in so doing, must flow in the $\hat{y}$ direction as it passes the connection points of the wires. Owing to the finite length of the leads, our choice of gauge is not of the London type, given that the vector potential is perpendicular to the short edges of the leads. Thus, the supercurrent along the short edges is determined by the component of the gradient of the phase $\nabla_y \phi$ that points along $\hat{y}$ direction. The expression for the current is $\vec{J}(x,y) = J_y\,\hat{y} = (t_f\,\phi_0/2\pi\mu_0\,\lambda^2)(\nabla_y\,\phi)\hat{y}$. If we now assume that, due to current conservation, we have $J_y = J_x$ then we may conclude that $\nabla_y \phi = (2\pi/\phi_0)Bl$. Correspondingly, the phase difference between the ends of the wires, which are separated by a distance $2a$, is $\delta(B) = \nabla_y\,\phi 2a = (2\pi/\phi_0)2alB$.

No we explain how the resistance oscillation period ΔB is calculated for the N-SQUID. First, we note that the phase accumulated around the loop formed by the wires and the electrodes is $\Delta\phi_{\rm loop} = \Delta\phi_{\rm w1} + \Delta\phi_{\rm w2} + 2\delta(B)$, where the quantities $\Delta\phi_{\rm w1}$ and $\Delta\phi_{\rm w2}$ correspond to the phase drops on the first and the second wires. The phase difference introduced by the electrodes, $\delta(B)$, appears in this expression with a factor 2, due to the fact that each of the electrodes generates the phase difference δ.

6.3 Resistance Oscillation Period

To calculate the period of the resistance oscillation we recall that the process considered here is a fluctuation process, involving multiple phase slips occurring on each wire, stochastically, at a frequency much higher than our data-acquisition frequency. The measured resistance of the device is proportional to the number of LPS crossing both wires per second. Each phase slip in a single wire corresponds to the entrance of a vortex into the loop, with the corresponding phase jump being

$\Delta\phi_{\rm loop} \rightarrow \Delta\phi_{\rm loop} + 2\pi$ (or $\Delta\phi_{\rm loop} \rightarrow \Delta\phi_{\rm loop} - 2\pi$ if it is an anti-vortex that enters the loop). Then, the vortex leaves the loop by crossing the second wire, thus accomplishing the elementary dissipative event.

To facilitate further discussion we introduce the following nomenclature: a state of the system with n vortices present in the loop (n is an integer number) and a phase difference imposed between the wires by the leads of 2δ, will be denoted $|n, 2\delta\rangle$. Note that the number of vortices is defined naturally as $n = \Delta\phi_{\rm loop}/2\pi$. For example, if the external field is zero and the number of vortices in the loop is zero then the state would be $|0, 0\rangle$. A state $|1, 2\pi\rangle$ would represent a situation in which there is one vortex in the loop and the external field imposes a phase shift of π between the pair of points on each electrode at which the wires are connected to the electrodes. Now let us compare two states of the system, viz., $|0, 0\rangle$ and $|1, 2\pi\rangle$. Both of them are equilibrium states, as each of them corresponds to zero supercurrent flowing through the wires, and thus they correspond to zero kinetic energy of the condensate in the nanowires. To see this, remember that by definition $\Delta\phi_{\rm w1} + \Delta\phi_{\rm w2} = \Delta\phi_{\rm loop} - 2\delta(B)$. If the wires are identical then the phase drop along each wire is the same. If the phase drop along each wire is $\Delta\phi_{\rm w}$ then we have $\Delta\phi_{\rm w1} = \Delta\phi_{\rm w2} = \Delta\phi_{\rm w}$, and so $\Delta\phi_{\rm w} = \Delta\phi_{\rm loop}/2 - \delta(B)$. For both states under consideration, we obtain $\Delta\phi_{\rm w} = 0$. In the first case, $|0, 0\rangle$, this is true because the phase-gradient introduced by the leads is zero and also the supercurrent from vortices trapped in the loop is zero (as there are no trapped vortices). Here, we note that we are assuming that the bias current flowing from one electrode to the other is negligibly small. In the second case, $|1, 2\pi\rangle$, the phase difference introduced by the electrodes is $2\delta = 2\pi$, whilst the phase-difference due to a single trapped vortex is also 2π. Therefore, the corresponding pair of

phase gradients cancel one another. The states of the type $|0, 0\rangle$ or $|1, 2\pi\rangle$ or, more generally, of the type $|n, 2\pi n\rangle$) are not frustrated, because they correspond to zero supercurrent in the wires and, therefore, to the lowest possible kinetic energy of the condensate in the wires. Note that these non-frustrated states are the most stable against fluctuations; they therefore correspond the the lowest rate of phase slips and, hence, the the lowest ohmic resistance. Thus, we see that the $R(B)$ curve should be periodic, with the lowest resistances being achieved at $2\delta = 2\pi n$. Consequently, the estimated period of the $R(B)$ oscillations is $\Delta B = \phi_0/4al$. The precise expression, obtained by solving the Laplace equation in the leads, gives a very similar result, viz., $\Delta B_{\text{theory}} = (\pi^2/8G)(\phi_0/4al)$. Put simply, the period defines the "distance" (in terms of the magnetic field) between the neighboring non-frustrated states. Note that states of the type $|n, 2\pi x\rangle$ with x being non-integral are frustrated, in the sense that no choice of the number of vortices in the loop can give zero supercurrent in the wires. These frustrated states are less stable, undergo more phase slips (because the supercurrent flowing through the wires suppresses the barrier for phase slips), and exhibit higher electrical resistance. This model quantitative explains the observed values of the oscillation period and qualitatively explains the observed oscillation in the $R(B)$ curves of Figure 11. The exact fits to the $R(B)$ curves have been computed by a more detailed theoretical analysis.[51]

6.4 Critical Switching and Retrapping Currents in N-SQUIDS

Examples of $V(I)$ curves for a sample with one wire are shown in Figure 7. The $V(I)$ curves for double-wire samples have the same shape. At lower temperatures, the $V(I)$ curves are hysteretic, and a jump-wise transition between the low-voltage state and the Joule-heated normal state (JNS) is observed at a current known as

the switching current $I_{\rm SW}$. The switching current is somewhat smaller than the depairing current of the wire, due to the effect of premature switching, initiated either by thermal or quantum fluctuations.[30] A detailed discussion of the difference between the depairing current and the sitching current will be given below, in the "Evidence for macroscopic quantum tunneling" section. The retrapping current $I_{\rm R}$ is the current at which the wire switches from the normal state back to the superconducting state. Roughly speaking, $I_{\rm R}$ is the current at which the Joule-heating power is no longer sufficient to keep the temperature of the wire above its current-reduced critical value. Experiments show[41] that $I_{\rm R}$ is weakly dependent on T, whilst $I_{\rm SW}$ shows a strong temperature dependence. Also, the value of $I_{\rm SW}$ exhibits a significant fluctuation ($\sim 50\,{\rm nA}$) from one measurement to the next, whereas the retrapping current is always the same, to within the precision of the measurement, which is typically $\sim 0.5\,{\rm nA}$. These differences between $I_{\rm SW}$ and $I_{\rm R}$ are due to the fact that the switching from the superconducting state to the JNS is effectively governed by the dynamics of a small number of weakly interacting degrees of freedom (owing to the presence of strong superconducting correlations), and thus is subject to strong thermal (or quantum) fluctuations. On the contrary, the switching from the normal state to the superconducting regime is governed by a macroscopic number of degrees of freedom, essentially corresponding to individual normal electrons in the wire. Correspondingly, the fluctuations are not detectable in the experiment, due to mutual averaging amongst the many degrees of freedom.

In a double-wire device, as the magnetic field is swept $I_{\rm SW}$ shows periodic oscillations, whilst the retrapping current is field-independent. This fact is illustrated in Figure 12. In this figure, the orange region corresponds to the superconduct-

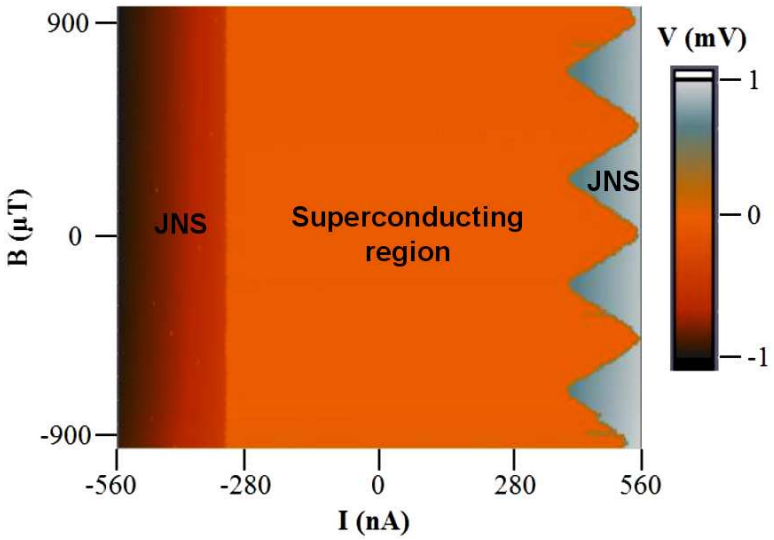

Figure 12: Dependence of the switching and retrapping currents on the magnetic field.[39]

ing regime of the N-SQUID (with the voltage being below the noise floor of the setup), whilst the gray area on the right and the dark area on the left represent the normal state (i.e., the JNS). The switching-current behavior is represented by the borderline between the orange and gray regions. This borderline, $I_{\mathrm{SW}}(B)$, exhibits periodic oscillations with magnetic field, with a period equal to the period of the $R(B)$ curve. The shape of the $I_{\mathrm{SW}}(B)$ curve is not sinusoidal, indicating that the current-phase relation (CPR) of the nanowire is not sinusoidal; this is different from the case of Josephson junctions, which have an essentially sinusoidal CPR. The boundary between the dark and the orange region, observed at negative bias current (see Figure 12), represents $I_{\mathrm{R}}(B)$ and appears to be a straight line. This absence of any field dependence proves that the darker region is indeed completely normal, and does not correspond to phase-slip-center behavior, which is what is more typically observed in thin superconducting wires at high bias current.[52] The occurrence of the normal state might be due to the fact that the wires are suspended,

and thus the heat generated by a phase slip center can easily heat the wire to above its critical temperature, leading to the realization of a completely normal state.

7 Evidence for Macroscopic Quantum Tunneling

Quantum behavior involving macroscopic degrees of freedom—i.e., physical variables describing large ensembles of particles—represents one of the most exciting fields of modern physics. A simple example of a macroscopic degree of freedom is the position of the center of mass of a large object, say a C_{60} molecule.[53] Initiated by Leggett more than 25 years ago,[54] research on macroscopic quantum tunneling (MQT) has undergone widespread development. Important settings for realizing MQT phenomena include such diverse systems as superconductor-insulator-superconductor (SIS) Josephson junctions,[55] and magnetic nanoparticles.[56]

The recognition of the advantages of quantum computers[57] has motivated the search for viable implementations of quantum bits, or qubits, several of which employ MQT in superconducting systems.[58] Interestingly, it has also been proposed that superconducting nanowires, if MQT occurs in them, could provide a possible setting for realizing novel qubits with improved decoherence properties.[59]

Also, substantial evidence has accumulated to indicate that MQT can occur in thin metallic wires of rather homogeneous cross section (see Ref.[60] and references therein). In nanowires, the MQT phenomenon is referred to as quantum phase slips (QPS). The occurrence of QPS implies that the wire is never truly superconducting: its resistance does not approach zero even when the temperature does. Thus, evidence for QPS is usually sought via the observation of a nonzero resistance at temperatures much lower than the critical temperature of the wire. Typically, one

concludes that QPS are present if $R(T)$ is flat at low temperatures, or if R drops with cooling slower than what might be expected from the thermal activation law $R \sim \exp(-\Delta F/k_{\rm B}T)$. On the other hand, our *short* wires made of MoGe did show strong evidence in favor of the existence of a true superconducting regime,[16] i.e., a regime without QPS, in which $R \sim \exp(-\Delta F/k_{\rm B}T)$. Note that at $T > 0$, the resistance is greater than zero in any model, as some LPS thermal activation is inevitable unless $T = 0$. The question that is not completely clear is whether or not signatures of MQT can be observed in *short* MoGe wires. (Empirically, "short" is defined as being shorter than $\sim 250\,{\rm nm}$.)

The possibility of MQT in superconducting junctions having insulating barriers has been clearly demonstrated experimentally (see Ref.[40] and references therein). This was achieved by exposing the samples to microwave radiation, and observing the discrete nature of the allowed energy states of the entire device, as one expects for a quantum system. More precisely, the microwaves were able to excite the system from the ground state to the next level, but only if the level spacing was equal to the energy of the photons of the applied radiation. Thus, it was possible to study the discrete energy states. Excitation of the system was detected through the premature switching (due to MQT) of the device from the superconducting to the normal state.

Recent experiments by Sahu et al.[28] give new evidence for MQT in homogeneous superconducting wires. This evidence for MQT is obtained by analyzing switching events, which occur at high bias currents, close to the depairing current. Below, we shall show how a detailed analysis of the statistics of the superconductor-to-normal switching currents can provide an affirmative answer to the question of whether or not QPS can occur in nanowires. The main point of argument is that at

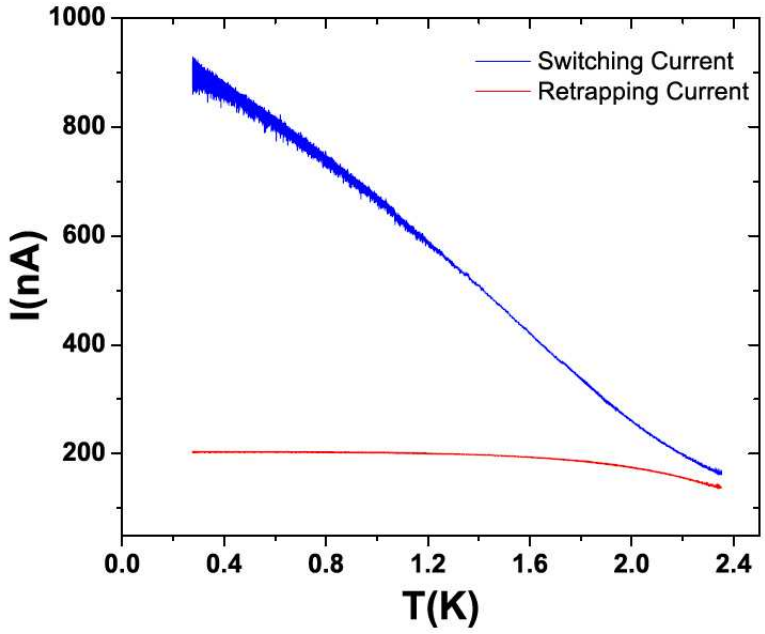

Figure 13: The upper curve (blue) shows the result of repeated switching current measurements as the temperature is varied. It illustrates the increase in fluctuations of I_{SW}, as the temperature is lowered. The lower curve (red) represents the measured I_{R} values, which show no fluctuations beyond the instrumental noise of the setup. In other words, the width of the lower curve provides a high-limit estimate of the current noise of the setup.[41]

low temperatures ($T \sim 300\,\mathrm{mK}$) the fluctuations of the value of the I_{SW} are much larger than the value expected on the basis of thermal fluctuations, and can be directly linked to QPS, which are a manifestation of quantum fluctuations. Thus, it is found that, although short MoGe wires do not exhibit QPS at low bias-currents, signatures of QPS do appear at high bias-currents near the depairing current, via the statistics of the premature switching events.[30]

7.1 Strong Fluctuations of the Value of the Switching Current

The switching current plotted in Figure 13 shows very pronounced fluctuations, much stronger than the instrumental noise. The values of I_{SW} and I_{R} have been

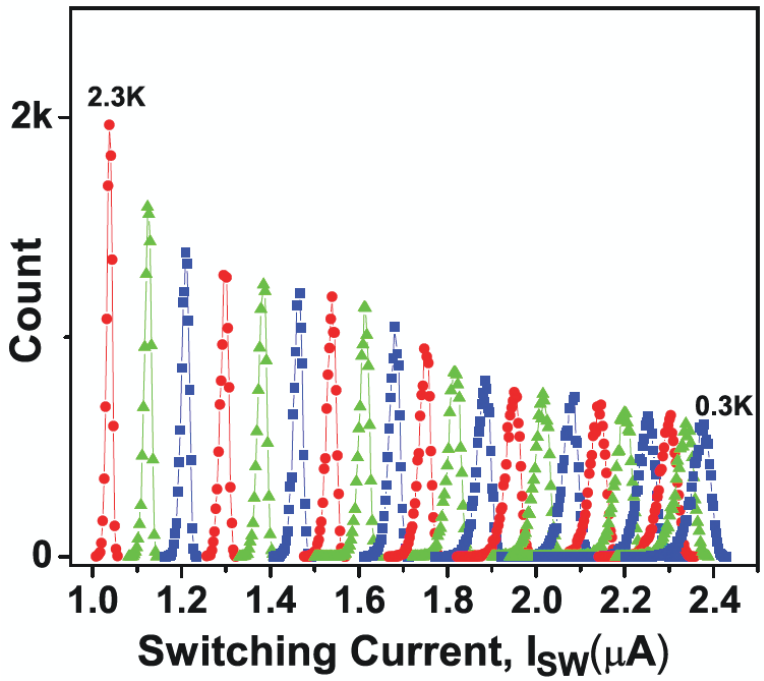

Figure 14: Switching current distributions for sample S1. The distributions are presented for 21 different temperatures in the range between $T = 0.3\,\mathrm{K}$ (right-most) and $T = 2.3\,\mathrm{K}$ (left-most), with a step size of $\Delta T = 0.1\,\mathrm{K}$. The parameters of the sample were the length $L = 110\,\mathrm{nm}$ and the normal resistance $R_\mathrm{N} = 2.67\,\mathrm{k\Omega}$. To get the distribution at each temperature the current was swept 10^4 times, starting from zero up to a high value, above the switching current. The exact value of the current at which the switching events occurred was recorded for each of the 10^4 sweeps. The histogram is plotted by choosing the bin size to be $\Delta I = 3\,\mathrm{nA}$. The vertical axis can be expressed as $Count = (10^4)\,(P(I_\mathrm{SW}))\,(\Delta I)$, where 10^4 is the number of measurements and $P(I_\mathrm{SW})$ is the probability density for the device to switch to the normal state when the bias current has the value I_SW.[28,41]

measured many times and plotted versus temperature. The upper curve (blue) shows that the amplitude of the fluctuations becomes larger as the temperature is reduced. To characterize the fluctuations of $I_{\rm SW}$ quantitatively, the temperature was fixed and the $V(I)$ curve was measured ten thousand times. For each $V(I)$ curve, the value of $I_{\rm SW}$ value was determined by finding the current at which the voltage exceeded the noise floor ($\sim 10\,\mu$V) by about one order of magnitude. As the voltage jump at the switching current is very strong, the results were independent on the precise choice of the threshold voltage. The results of such an analysis, for various temperatures, are shown in Figure 14. There, we can see that, as we increase the value of T (in the interval $0.3\,{\rm K} < T < 2.3\,{\rm K}$), the distributions of the switching currents become narrower (and correspondingly taller, as the area, which represents the total number of measurements, is the same for all curves). The vertical axis of Figure 14, marked "Count," can be expressed as Count $=$ $10^4 * P(I_{\rm SW}) * \Delta P$, where 10^4 is the number of measurements at each temperature, $P(I_{\rm SW})$ is the probability density for the measured value of the switching current to be $I_{\rm SW}$, and ΔP is the bin size chosen for plotting the distributions. Figure 15 shows how the effective width of the distribution (i.e., the standard deviation of the measured set of switching currents $\sigma = \sqrt{\sum_{i=1}^{n}(I_{{\rm SW},i} - \overline{I_{\rm SW}})^2/(n-1)}$) varies as a function of temperature for samples S1 to S5. These samples were fabricated as is illustrated in Figure 1a. The only difference between them is that S5 is made thicker and it has a larger critical current (the values of the critical current are given in the caption to Figure 15). In this definition, $I_{{\rm SW},i}$ represents the 10^4 measured data points for the switching current, whilst $\overline{I_{\rm SW}}$ is the corresponding mean value. We find that (1) the standard deviation (i.e., the fluctuation strength) increases with decreasing temperature, and (2) the samples having larger critical

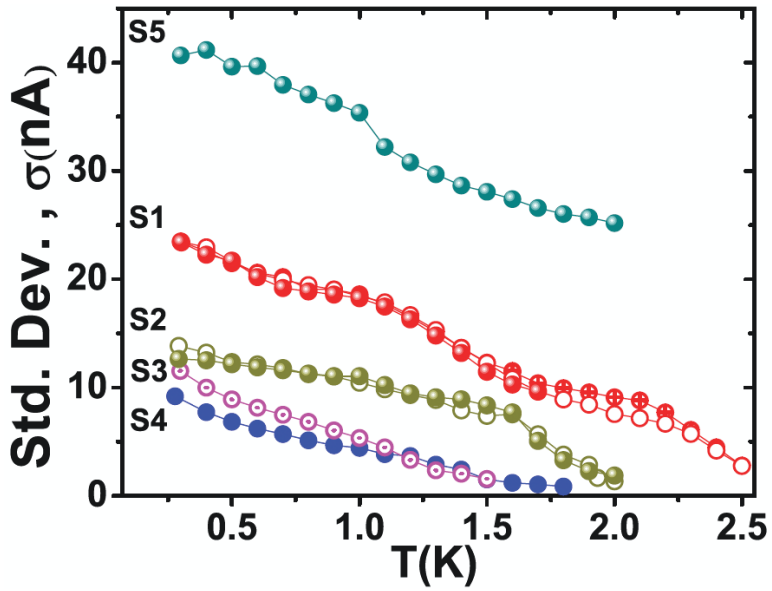

Figure 15: Temperature dependence of the standard deviation of the switching current distribution, plotted versus temperature, for five different samples.[41] The measurements for samples S1 and S2 were repeated more than once, in order to verify their reproducibility. The corresponding values of the critical depairing current for samples S1 to S5 are $I_{\rm C}(0) = 2.92, 1.72, 1.68, 1.10, \text{ and } 6.16\,\mu$A. The values of the critical current are obtained via a fitting procedure explained in the text.[28,41]

currents are characterized by larger values of σ.

It should be emphasized that the observed broadening of the distributions with cooling is, in general, unexpected, as thermal fluctuations, presumably causing the fluctuations in the $I_{\rm SW}$ values, would become weaker with cooling. Note that measurements on SIS Josephson junctions do indeed show just such a trend: the fluctuations became weaker with cooling.[40,61]

7.2 Extracting Switching Rates

Further understanding of the statistics of the switching events can be achieved by applying the analysis of Fulton and Dunkleberger (FD).[61] First, we note that the

values of σ introduced above, as well as the exact shape of the $P(I_{SW})$ curves (Figure 14), are not universal. They depend on the bias current sweeping rate dI/dt chosen during the measurements of the switching events. The general rule is this: The faster the sweeping rate, the smaller the difference between $\overline{I_{SW}}$ and the depairing current of the wire $I_{\rm C} = I_{\rm C}(T)$. In the limit $dI/dt \to \infty$, the premature switching does not have time to happen, and the distribution function becomes a Dirac δ-function centered at $I_{\rm C}(T)$, viz., $P(I_{\rm SW}) = \delta(I_{\rm C}(T) - I_{\rm SW})$, and also $\sigma = 0$. The depairing current is the current at which the superconductivity breaks down with certainty because the superconducting state free energy becomes larger than the free energy of the normal state. Therefore, $P(I) = 0$ for $I > I_{\rm C}(T)$.

The FD analysis allows one to convert the sweep-rate-dependent distribution function $P(I_{\rm SW})$ into the sweep-rate-independent switching rate function $\Gamma(T, I)$. The analysis is based on the relation

$$P(I)dI = \Gamma(I)(dI/dt)^{-1}dI \left(1 - \int_I^0 P(I')dI'\right), \tag{6}$$

where $P(I)dI$ is the probability that the device switches to the normal state in the interval between bias currents I and $I + dI$, $(dI/dT)^{-1}dI$ is the duration of time during which the bias current belongs to the interval between I and $I + dI$, $\Gamma(I)$ is the switching rate (i.e., the average number of switching events that the system would undergo if the bias current would be fixed at I), and the expression $\left(1 - \int_0^I P(I')dI'\right) = \int_I^{I_C} P(I')dI'$ gives the probability that the current is swept from zero to I without switching.

In general, the sweeping rate can be a function of the value of the current. For example, if the bias current has a sinusoidal time dependence $I(t) = I_a \sin(\omega t)$ then the sweeping rate is given by $dI/dt = I_a\omega\cos(\omega t) = I_a\omega\sqrt{(1 - (I/I_a)^2}$,

where I_a is the amplitude of the bias current, which must satisfy $I_a > I_{\rm C}(T)$. In the experiment,[28] a triangular sweeping function was used, such that $I_a = 2.75\,\mu$A and $dI/dt = 125.5\,\mu{\rm A/s}$.

As, in practice, the histogram is expressed in digital format, the expression for the switching rate needs to be expressed in terms of finite sums rather than integrals. Let the current axis be split into bins of size ΔI and the corresponding current values be numbered $I_k = I_{\rm C} - k\Delta I$, where the integer bin number k obeys $0 < k < N$, with the highest bin number N defined via $N = I_{\rm C}/\Delta I$. This type of definition implies that bin number zero corresponds to $I = I_{\rm C}$ and the higher numbers correspond to lower currents. Then the switching rate can be expressed as:[61]

$$\Gamma_k = \Gamma(I_k) = \frac{dI}{dt}(1/\Delta I)\ln\left(\frac{\sum_{i=0}^{k} P(I_i)}{\sum_{i=0}^{k-1} P(I_i)}\right) \tag{7}$$

7.3 Correspondence Between Switching Events and Phase Slips

The results of the FD-type analysis are shown in Figure 16 for a measurement done at a low temperature, viz., at $T = 300\,{\rm mK}$. The open circles represent the dependence of the switching rate on temperature, and the continuous curves represent different models. The best fit is provided by the QPS model, whilst the models involving only thermal fluctuations and neglecting quantum fluctuations (to be called TAPS models, the abbreviation standing for "thermally activated phase slips") do not agree with the data at all.

In order to obtain the fits of Figure 16 we have to make an assumption about the relationship between single phase slips (whether thermally activated or quantum) and the switching events observed in the experiment. The simplest assumption is that a single phase slip corresponds to every switching event. Under such hypoth-

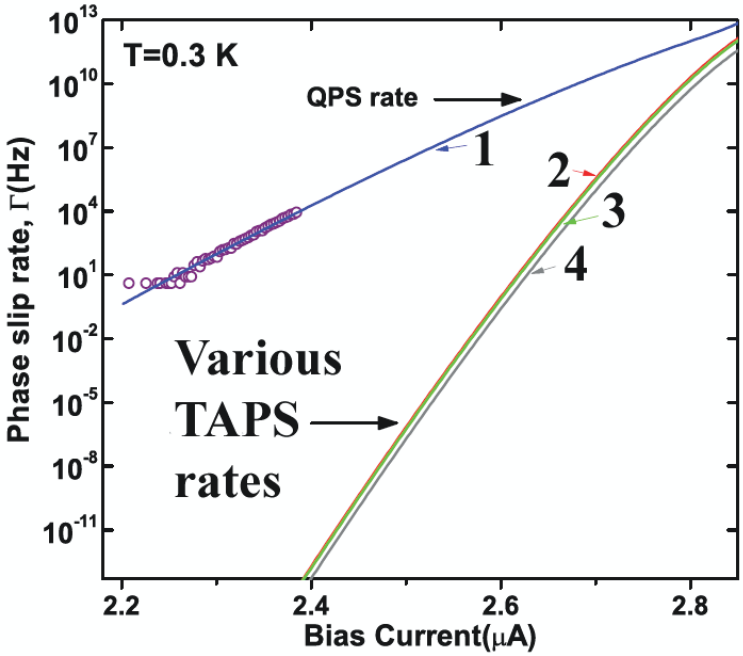

Figure 16: The experimental switching rate (open circles) and the calculated QPS rate (solid blue line) are shown for $T = 0.3$ K for the sample S1. The observed agreement is very good. Various estimates of the TAPS rate by using different attempt frequency expressions are also shown by solid red, green, and gray lines. For all estimates of the TAPS rate, the experimental values are at least 10^{17} orders of magnitude higher than the calculated thermal rate. Hence, the data can not be explained by considering thermal fluctuation alone, even if the uncertainty in the attempt frequency is taken into account.[28,41]

esis, as the current is increased the wire initially remains fully superconducting (i.e., it shows zero voltage even though the current is greater than zero) until a single TAPS or QPS occurs. As soon as a single phase slip happens, it dissipates the kinetic energy of the supercurrent in the wire as heat. The heat dissipated as a result of a single LPS is $\Delta E_{LPS} = hI/2e$. Note that the released heat is proportional to the bias current. A detailed analysis of the heating effect in suspended wires, due to Shah et al.,,[62] shows that if the temperature is sufficiently low (and $T = 300\,\mathrm{mK}$ was sufficiently low for our samples), the dissipated energy ΔE is sufficient to increase the temperature of the wire above its current-dependent critical temperature $T_{\mathrm{C}}(I)$. To understand why at low temperatures a single LPS is sufficient to increase the temperature of the wire above $T_{\mathrm{C}}(I)$ while at higher temperatures a single LPS is not sufficient we first remind the fact that LPS are less frequent at low temperatures for a given value of the LPS barrier. Thus, as the current is slowly increased, the wire stays LPS-free until the current is very near the depairing current. Therefore, the first phase slip occurs when ΔE_{LPS} is high and $T_{\mathrm{C}}(I)$ is low. That is why one LPS is sufficient to overheat the wire at low temperatures, whereas it is not sufficient at higher temperatures, since at higher temperatures the LPS start to occur with an appreciable frequency even at low bias current a which $E_{LPS} = hI/2e$ is not sufficient to overheat the wire. If this happens, the wire becomes normal, at least for a short time, until the dissipated heat has enough time to flow away from the nanowire. (This typically takes some nanoseconds.) As the current through the wire I is set by an external current source, the current keeps flowing even if an LPS makes it temporarily nonsuperconducting. The additional Joule heating generated due to the current passing through a nonsuperconducting region of the wire leads to further, rapid growth of

the temperature, which eventually leads to the observable switching event. Thus, the statistics of the switching events is in one-to-one correspondence with the statistics of phase slips. In order to explain these stochastic features quantitatively, we review below the formulas describing the rates of QPS and TAPS.

7.4 Rates of Phase Slips

The rate of TAPS is given by the Arrhenius-type expression[30]

$$\Gamma_{\mathrm{TAPS}} = (\Omega_{\mathrm{TAPS}}/2\pi)\exp(-\Delta F/k_{\mathrm{B}}T). \tag{8}$$

By analogy, the rate of quantum phase slips can be estimated as

$$\Gamma_{\mathrm{QPS}} = (\Omega_{\mathrm{QPS}}/2\pi)\exp(-\Delta F/k_{\mathrm{B}}T_{\mathrm{Q}}), \tag{9}$$

which was justified by Giordano[45] and Lau et al.[34] Here, T_{Q} is an effective temperature characterizing the strength of quantum fluctuations.[40] If the device under consideration contains a superconducting wire that links two macroscopic electrodes (as is the case in the experiments discussed in the Progress Report), the kinetic inductance of the wire is given by[63] $L_{\mathrm{K}} = (L/\xi(T))\hbar/3\sqrt{3}eI_{\mathrm{C}}$, and the electrical capacitance between the electrodes is C_{E}, then the quantum temperature can be roughly estimated as $T_{\mathrm{Q}} = (\hbar/k_{\mathrm{B}})/\sqrt{L_{\mathrm{K}}C_{\mathrm{E}}}$.

To analyze data at temperatures well below T_{C}, we estimate the barrier for phase slips by combining Eqs. (2,3,4). The result is a formula that is valid, to a good approximation, over a wide temperature range:

$$\Delta F(T) = \big(\sqrt{6}(\hbar/2e)\big)0.83k_{\mathrm{B}}T_{\mathrm{C}}(R_{\mathrm{Q}}/R_{\mathrm{N}})(L/\xi(0))\big(1-(T/T_{\mathrm{C}})^2\big)^{3/2}. \tag{10}$$

In order to make fits to the experimentally obtained switching rates, one needs to know how the barrier for the LPS changes with the bias current. The corresponding

formula is[43]

$$\Delta F(I,T) = \Delta F(0,T)\,(1 - I/I_{\rm C}(T))^{5/4}\,, \tag{11}$$

where $\Delta F(0,T)$ is the barrier energy to phase slip at zero current and a given temperature. It is worth noting that the corresponding expression for the more thoroughly studied case of a Josephson junction has the same form,[30] but an exponent of 3/2 instead of 5/4. Qualitatively, the two cases are very similar.[43]

The attempt frequency for the QPS can be plausibly estimated from the LAMH attempt frequency, Eq. (1), by replacing the thermal energy $k_{\rm B}T$ by an effective quantum energy. In Ref.,[28] the choice was made to make the following replacement in the LAMH expression for the attempt frequency: $\Delta F/k_{\rm B}T \rightarrow \Delta F/k_{\rm B}T_{\rm Q}$. There is no rigorous justification for such replacement. But, fortunately, the choice of the attempt frequency is not important, as the expression for the switching rate is always dominated by the exponential factor, as we shall discuss below. The QPS attempt frequency thus becomes:

$$\Omega_{\rm QPS} = \big(8k_{\rm B}(T_{\rm C} - T)/\pi\hbar\big)\big(L/\xi(T)\big)\sqrt{\pi\Delta F(T)/k_{\rm B}T_{\rm Q}}. \tag{12}$$

The QPS switching rate computed using Eqs. (9,10,11,12) is plotted in Figure 16 versus the bias current (see the blue curve, marked #1). The fitting parameters used are $T_{\rm Q} = 0.85\,{\rm K}$, $T_{\rm C} = 3.87\,{\rm K}$, and $\xi(0) = 5\,{\rm nm}$. The parameters known from independent measurements are the normal resistance and the sample length, viz., $R_{\rm N} = 2.67\,{\rm k}\Omega$ and $L = 110\,{\rm nm}$. The calculated rate is in a good agreement with the data. Thus, the hypothesis that QPS control the observed strong fluctuations of the switching current finds significant justification. Additional justification comes from the fact that $T_{\rm Q}$ was observed to become greater in wires of larger diameter, which have higher critical currents.[28] If the observed strong fluctuations of $I_{\rm SW}$

were due to some trivial reason, such as an excess electromagnetic noise in the setup leads, or granularity in the wires, then one would expect to see a smaller $T_{\rm Q}$ in thicker wires. This is because thicker wires would, presumably, be less susceptible to problems such as electromagnetic noise or granularity of the wire. In reality, larger $T_{\rm Q}$ values were found in thicker wires.[28]

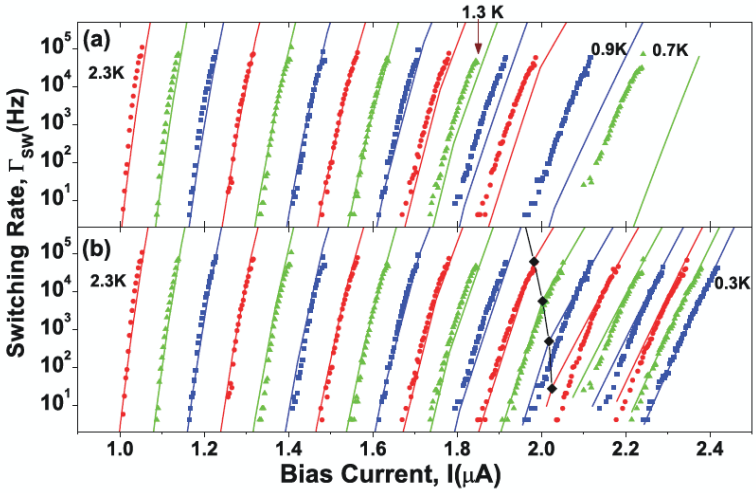

Figure 17: (a) Switching rates from the superconducting state to the resistive state for bath temperatures between $2.3\,\mathrm{K}$ (left most) and $0.7\,\mathrm{K}$ (right most). (For the sake of clarity, not all the measured curves are shown here.) The data is shown for all temperatures between $2.3\,\mathrm{K}$ and $1.1\,\mathrm{K}$ with $\Delta T = 0.1\,\mathrm{K}$ as well as for $T = 0.9\,\mathrm{K}$ and $T = 0.7\,\mathrm{K}$ (sample S1). The symbols are experimental data and the lines (with corresponding colors) are fits to the overheating model, incorporating stochastic TAPS-only events.[28,62] The fits agree well with the data down to $T = 1.3\,\mathrm{K}$, which is indicated by an arrow. (b) Fits to the same data (all temperatures are shown here) with the stochastic overheating model but now incorporating both TAPS and QPS rates. The boundary for the single phase-slip-switching regime is indicated by the black diamond symbols, connected by line segments, for four temperatures. The single-phase-slip switching regime occurs to the right of the line connecting the diamonds.[41]

On the other hand, curves 2, 3 and 4 (see Figure 16) all represent the TAPS model, given by Eq. 8. The reason we show three curves is that in this model the attempt frequency is not well established, except very near $T_{\rm C}$.[47] In the

case of curve #2, LAMH theory was followed and the assumption was made that $\Omega_{\mathrm{TAPS}} = \Omega_{\mathrm{LAMH}}$ (see Eq. 1). Curve #3 (green) is plotted using a modified attempt frequency. The new expression is obtained by using Eq. 1 and making the replacement $1/\tau_{\mathrm{GL}} \rightarrow \omega_{\mathrm{p}}$, where $\omega_{\mathrm{p}} = \sqrt{2eI_{\mathrm{C}}(T)/\hbar C_{\mathrm{E}}}$ is the so-called plasma frequency of a Josephson junction. Curve #4 (gray) is again obtained using Eq. 1 but now making the replacement $1/\tau_{\mathrm{GL}} \rightarrow \omega_{\mathrm{w}}$, where $\omega_{\mathrm{w}} = 1/\sqrt{L_{\mathrm{K}}C_{\mathrm{E}}}$ is the analog of the plasma frequency for a system having a nanowire. Apparently, none of the TAPS expressions tested can fit the data. Also it is clear that the exponential factor dominates over the pre-exponential attempt frequency. In other words, any tested choice of the attempt frequency gives almost the same result: the curves 2, 3 and 4 are very close to one another. This gives evidence that, as with TAPS, the choice of the attempt frequency for QPS is not essential and need not be known precisely.

Finally, a general model was developed, which takes into account both TAPS and QPS. The model also takes into account the fact that at higher temperatures a single LPS is not sufficient to cause a switching event.[28,62] On the contrary, the model predicts that, at higher temperatures, many phase slips must occur almost simultaneously in order to overheat the wire and switch it into the JNS.[28,62] This conclusion is directly confirmed by the fact that the $V(I)$ curves measured at higher temperatures (i.e., close to T_{C}) show nonzero voltages before the switch to the JNS occurs. For example, on sample S1 such a pre-switching "voltage tail" was observed down to $T \approx 2.5\,\mathrm{K}$.[28] This fact confirms that LPS occur before the switch. The results of the general model, in comparison to the experiment, are shown in (Figure 17). In Figure 17a the experimental switching rate was compared to a partial model, which includes only TAPS. It is clear that the model

of overheating with TAPS works well at higher temperatures, but fails to describe data below $T \sim 1\,\mathrm{K}$. Thus, one needs to bring QPS into consideration. The fitting curves in Figure 17b are computed by including both the TAPS and QPS switching rates. In this case, good agreement is observed over the entire temperature interval, down to $T = 0.3\,\mathrm{K}$. Thus, it is clear that the phenomenon of macroscopic quantum tunneling must be included in the model in order to obtain reasonable agreement with the data. We also note that the general overheating model[62] provides a natural explanation of the observed growth, as the temperature is reduced, in the fluctuations of I_{SW} (see Figure 15). The explanation is that a smaller and smaller number of LPS is required to overheat the wire as the temperature is reduced. Thus, the stochastic nature of the switching process becomes more pronounced.

8 Summary

In this Progress Report we have covered four main topics: (1) the molecular templating technique for making nanowires, (2) the transport properties of molecule-templated superconducting nanowires, (3) the fabrication and properties of double-wire SQUID devices, and (4) evidence for the occurrence of macroscopic quantum tunneling in nanowires at high values of the supercurrent.

The best molecules for fabricating nanowires turn out to be fluorinated single-walled carbon nanotubes. DNA has the disadvantage of being less rigid, compared to carbon nanotubes. Also, nanowires made with DNA tend to be somewhat larger in diameter, possibly because the DNA molecule has a larger diameter after being suspended and dried, due to the difficulty of removing all contamination surrounding the molecule. The potential advantage of DNA molecules, associated with their

ability to self-assemble into complex constructs having pre-designed geometries, has not, to date, been realized and employed for the fabrication of superconducting networks. This possibility remains for future research on molecule-templated devices. The idea would be to design and synthesize DNA molecules of well-defined sequences of base pairs, and to then allow these molecules to self-assemble into a network having a desired structural configuration. It is expected that such networks can be formed in a suspended state, and then coated with superconducting metal or alloy. Thus, a network of ultra-thing superconducting wires would be obtained. Such superconducting wire networks could be used for information processing, where the information bits are represented by different values of quantized supercoducting currents circulating around the cells of the network.

Transport measurements on thin superconducting wires confirmed the expected absence of a thermodynamic normal-to-superconductor phase transition. This absence is explicitly manifested by the fact the the resistance remains greater than zero at any nonzero temperature (although it does become smaller with cooling, and can fall below the sensitivity of the experimental setup). The resistance is governed by the Arrhenius law of thermal activation, the energy barrier of which is determined by the free energy required to convert a segment of the wire from the superconducting to the normal state.

By connecting two wires in parallel we were able to observe a new variant of quantum interference, which has an analogy with the famous double-slit experiment of quantum mechanics. In the present case, the phase difference between two interfering paths is induced by the Meissner screening currents that circulate in the electrodes, when the electrodes are pierced by an external magnetic field. These novel nanowire-SQUIDS can be used to measure local magnetic fields, as well as

to control critical currents in superconducting devices that involve nanowires.

Proving that MQT does indeed occur in thin superconducting wires is a formidable task. The difficulties arise because other factors can be easily mistaken for MQT. Our approach for showing the existence of MQT is based on a trigger effect that is related to the Joule-overheating of the wires. When a single phase-slip occurs, the temperature of the wire jumps, switching the wire to the normal state. Such switching events are easy to detect, in contrast with individual phase slips. The proof of the existence of MQT is based on our observations (i) that the fluctuations of the switching current are much larger than would be expected on the basis of thermal fluctuations at a given temperature, and (ii) that the observed fluctuations are larger in wires that have larger critical currents.

In the future, we plan to continue studies of MQT effects in thin wire devices. The next step will be to employ an environmental dissipation bath, possibly represented by a normal resistor, in order to control the rate of QPS, following the general ideas set forth by Leggett.[54]

Acknowledgments

The authors gratefully acknowledge many extensive and highly informative discussions on the topics reviewed here (as well as on related issues), which they have enjoyed with their colleagues and collaborators, especially D. Hopkins, A. J. Leggett, D. Pekker, G. Refael, A. Rogachev, M. Sahu, N. Shah, and T-C. Wei. They also gratefully acknowledge the use of fabrication facilities at the Frederick Seitz Materials Research Laboratory. This material is based upon work supported by the U.S. Department of Energy, Division of Materials Sciences under

Award No. DE-FG02-07ER46453, through the Frederick Seitz Materials Research Laboratory at the University of Illinois at Urbana-Champaign.

References

[1] J. D. Watson and F. H. C. Crick, *Nature* **1953**, *171*, 737.

[2] P. W. Rothemund, *Nature* **2006**, *440*, 297.

[3] E. S. Andersen, M. Dong, M. M. Nielsen, K. Jahn, R. Subramani, W. Mamdouh, M. M. Golas, B. Sander, H. Stark, C. L. Oliveira, J. S. Pedersen, V. Birkedal, F. Besenbacher, K. V. Gothelf, J. Kjems, *Nature* **2009**, *459*, 73.

[4] F. A. Aldaye, A. L. Palmer, H. F. Sleiman HF, *Science* **2008**, *321*, 1795.

[5] E. Braun, K. Keren, *Adv. Phys.* **2004**, *53*, 441.

[6] H. Watanabe, C. Manabe, T. Shigematsu, K. Shimotani, M. Shimizu, *Appl. Phys. Lett.* **2001**, *79*, 2462.

[7] N. C. Seeman, *Angew. Chem. Int. Ed.* **1998**, *37*, 3220.

[8] E. Braun, Y. Eichen, U. Sivan, G. Ben-Yoseph, *Nature* **1998**, *391*, 775.

[9] J. Richter, M.Mertig, W. Pompe, I. Monch, H. K. Schakert, *Appl. Phys. Lett.* **2001**, *78*, 536.

[10] 7. J. Richter, M. Mertig, W. Pompe, H. Vinzelberg, *Appl. Phys. A* **2002**, *74*, 725.

[11] M. Mertig, L. C. Ciacchi, R. Seidel, W. Pompe, *Nano Lett.* **2002**, *2*, 841.

[12] T.A. Fulton and G.J. Dolan, *Phys. Rev. Lett.* **1987**, *59*, 109.

[13] D.V. Averin and K.K Likharev in Mesoscopic Phenomena in Solids, edited by B.L. Altshuler, P.A. Lee, and R.A. Webb (Elsevier, Amsterdam, 1991).

[14] Single Charge Tunneling, edited by H. Grabert and M. H. Devoret (Plenum, New York, 1992).

[15] A. Bezryadin, C. N. Lau, and M. Tinkham, *Nature* **2000**, *404*, 971.

[16] A. T. Bollinger, R. C. Dinsmore, A. Rogachev, and A. Bezryadin, *Phys. Rev. Lett.* **2008**, *101*, 227003.

[17] Y. Zhang and H. Dai, *Appl. Phys. Lett.* **2000**, *77*, 3015.

[18] A. Bezryadin, A. Bollinger, D. Hopkins, M. Murphey, M. Remeika, and A. Rogachev, in Dekker Encyclopedia of Nanoscience and Nanotechnology, Editors: James A. Schwarz, Cristian I. Contescu, and Karol Putyera (Marcel Dekker, Inc. New York, 2004), p. 3761.

[19] M. Remeika and A. Bezryadin, *Nanotechnology* **2005**, *16*, 1172.

[20] A. Bezryadin, *J. of Phys. Condens. Matter* **2008**, *76*, 43202.

[21] D. Hopkins, D. Pekker, P. Goldbart, and A. Bezryadin, *Science* **2005**, *308*, 1762.

[22] D. S. Hopkins, D. Pekker, T.-C. Wei, P. M. Goldbart, and A. Bezryadin, *Phys. Rev.* B, *Rapid Comm.* **2007**, *76*, 220506(R).

[23] A. Rogachev and A. Bezryadin, *Appl. Phys. Lett.* **2003**, *83*, 512.

[24] J. M. Graybeal and M. R. Beasley, *Phys. Rev.* B **1984**, *29*, 4167.

[25] J. M. Graybeal, PhD Thesis, Stanford (1985).

[26] W. A. Little, *Phys. Rev.* **1967**, *156*, 396.

[27] K. Xu and J. R. Heath, *Nano Lett.* **2008**, *8*, 3845.

[28] M. Sahu, M.-H. Bae, A. Rogachev, D. Pekker, T.-C. Wei, N. Shah, P. M. Goldbart, and A. Bezryadin, *Nature Physics*, **2009**, *5*, 503.

[29] R. C. Jaklevic, J. Lambe, A. H. Silver, J. E. Mercereau, *Phys. Rev. Lett.* **1964**, *12*, 159.

[30] M. Tinkham, Introduction to Superconductivity (McGraw- Hill, New York, ed. 2, 1996).

[31] W. A. Little and R. D. Parks, *Phys. Rev. Lett.* **1962**, *9*, 9; *Phys. Rev.* **1964**, *133*, A97.

[32] A. Bezryadin and C. Dekker, *J. Vac. Sci. Technol. B* **1997**, *15*, 793.

[33] A. Bollinger, PhD Thesis, University of Illinois at Urbana-Champaign, 2005.

[34] C. N. Lau, N. Markovic, M. Bockrath, A. Bezryadin and M. Tinkham, *Phys. Rev. Lett.* **2001**, *87*, 217003.

[35] A. T. Bollinger, A. Rogachev, M. Remeika, and A. Bezryadin, *Phys. Rev.* B, *Rapid Communications* **2004**, *69*, 180503(R).

[36] K. F. Kelly, I. W. Chiang, E. T. Michelson, R. H. Hauge, J. L. Margrave, X. Wang, G. E. Scuseria, C. Radoff, and N. J. Halas, *Chem. Phys. Lett.* **1999**, *313*, 445.

[37] A. Johansson, G. Sambandamurthy, and D. Shahar, N. Jacobson and R. Tenne, *Phys. Rev. Lett.* **2005**, *95*, 116805.

[38] Y. Liu, Yu. Zadorozhny, M. M. Rosario, B. Y. Rock, P. T. Carrigan, H. Wang, *Science* **2001**, *294*, 2332.

[39] David Scott Hopkins, Ph.D.Thesis, University of Illinois at Urbana-Champaign, 2006.

[40] J. M. Martinis, M. H. Devoret, and J. Clarke, *Phys. Rev.* B **1987** *35*, 4682.

[41] M. Sahu, PhD Thesis, University of Illinois at Urbana-Champaign, 2009.

[42] Y. Oreg and A. M. Finkel'stein, *Phys. Rev. Lett.* **1999**, *83*, 191.

[43] M. Tinkham, J. U. Free, C. N. Lau and N. Markovic, *Phys. Rev.* B **2002**, *68*, 134515.

[44] D. E. McCumber and B. I. Halperin, *Phys. Rev.* B **1970**, *1*, 1054.

[45] N. Giordano, *Phys. Rev. Lett.* **1988**, *61*, 2137.

[46] J. S. Langer and V. Ambegaokar, *Phys. Rev.* **1967**, *164*, 498.

[47] D. Meidan, Y. Oreg and G. Refael, *Phys. Rev. Lett.* **2007**, *98*, 187001.

[48] S. L. Chu, A. T. Bollinger and A. Bezryadin, *Phys. Rev.* B **2004**, *70*, 214506.

[49] M. Tinkham and C. N. Lau, *Appl. Phys. Lett.* **2002**, *80*, 2946.

[50] J. Bardeen, *Rev. Mod. Phys.* **1962**, *34*, 667.

[51] D. Pekker, A. Bezryadin, D. S. Hopkins, and P. M. Goldbart, *Phys. Rev.* B **2005**, *72*, 104517.

[52] R. Tidecks, Current-induced Nonequilibrium Phenomena in Quasi-One-Dimensional Superconductors, Springer Tracts in Modern Physics Vol. 121 (Springer-Verlag, Berlin-Heidelberg, 1990).

[53] M. Arndt, O. Nairz, J. Voss-Andreae, C. Keller, G. van der Zouw, and A. Zeilinger, *Nature* **1999**, *401*, 680.

[54] A. J. Leggett, *J. Phys. Colloq.* **1978**, *39*, 1264; A. J. Leggett, *Prog. Theor. Phys. Suppl.* **1980**, *69*, 80; A. O. Caldeira and A. J. Leggett, *Phys. Rev. Lett.* **1981**, *46*, 211; A. J. Leggett, Lesson of Quantum Theory. N. Bohr Centenary Symposium, 35-57 (North-Holland, 1986); A. J. Leggett, S. Chakravarty, A. T. Dorsey, A. Garg, W. Zwerger, *Rev. Mod. Phys.* **1987**, *59*, 1.

[55] R. F. Voss and R. A., *Phys. Rev. Lett.* **1981** *47*, 265; K. Inomata, S. Sato, K. Nakajima, A. Tanaka, Y. Takano, H. B. Wang, M. Nagao, H. Hatano, and S. Kawabata, *Phys. Rev. Lett.* **2005**, *95*, 107005; A. Wallraff, A. Lukashenko, J. Lisenfeld, A. Kemp, M. V. Fistul, Y. Koval, and A. V. Ustinov, *Nature* **2003**, *425*, 155.

[56] W. Wernsdorfer, E. Bonet Orozco, K. Hasselbach, A. Benoit, D. Mailly, O. Kubo, H. Nakano, and B. Barbara, *Phys. Rev. Lett.* **1997**, *79*, 4014.

[57] P. Shor, Proc. 35th Annual Symposium on Foundations of Computer Science 124-134 (1994); P. Shor, *SIAM J. Computing* **1997**, *26*, 1484.

[58] A. Izmalkov, M. Grajcar, E. IlŠichev, Th. Wagner, H.-G. Meyer, A. Yu. Smirnov, M. H. S. Amin, A. M. van den Brink, and A. M. Zagoskin, *Phys. Rev. Lett.* **2004** *93*, 037003.

[59] J. E. Mooij and C. J. P. M. Harmans, *New J. Phys.* **2005**, *7*, 219.

[60] K. Yu. Arutyunov, D. S. Golubev, A. D. Zaikin, *Phys. Rep.* **2008**, *464*, 1.

[61] T.A. Fulton and L. N. Dunkleberger, *Phys. Rev.* B **1974**, *9*, 4760.

[62] N. Shah, D. Pekker, and P. M. Goldbart, *Phys. Rev. Lett.* **2008**, *101*, 207001; and D. Pekker, N. Shah, M. Sahu, A. Bezryadin, and P. M. Goldbart, *Stochastic dynamics of phase-slip trains and superconductive-resistive switching in current-biased nanowires*, arXiv:0904.4432v1 [cond-mat.supr-con].

[63] K. K. Likharev, *Rev. Mod. Phys.* **1979** *51*, 101.

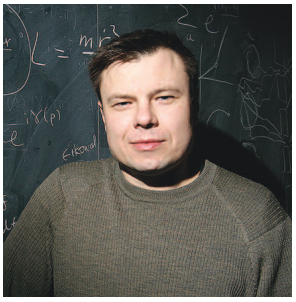

Figure 18: *Alexey Bezryadin received his B.Sc. and M.Sc. degrees in Physics and Applied Mathematics from Moscow Institute of Physics and Technology, Russia, in 1990. He received his doctorate in Physics from Joseph Fourier University in Grenoble, France, in 1995. He was a postdoctoral researcher at Delft University of Technology in the Netherlands (1995-1997) and at Harvard University, U.S.A. (1997-2000). He joined the Physics Department of the University of Illinois at Urbana-Champaign, U.S.A., in 2000, where he currently holds the positions of Associate Professor of Physics and Research Professor in the Frederick Seitz Materials Research Laboratory.*

Figure 19: *Paul Goldbart received his B.A. degree in Physics and Theoretical Physics from the University of Cambridge, U.K., in 1981, and his M.S. degree in Physics from the University of California–Los Angeles, U.S.A., in 1982. He received his doctorate in Physics from Imperial College of Science and Technology, University of London, U.K., in 1985. He joined the Department of Physics at the University of Illinois at Urbana-Champaign, U.S.A., in 1985 as a postdoctoral researcher, becoming an assistant professor in 1987; he currently holds the positions of Professor of Physics, Director of the Institute for Condensed Matter Theory, and Research Professor in the Frederick Seitz Materials Research Laboratory.*

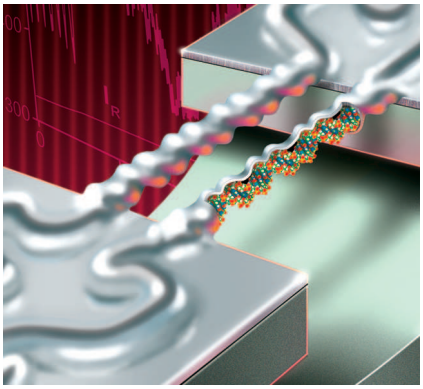

Figure 20: The Table of Contents Entry: Two DNA molecules are placed across a trench etched into a SiN-coated substrate. The DNA molecules dry, and after the drying they are found to be suspended between the banks of the trench and perfectly straight. Such suspended DNA molecules are subjected to metal coating by sputtering. The metallization is done by sputter-deposition of a few nanometer film of an amorphous alloy of MoGe, which is superconducting. Thus each suspended DNA is transformed into a superconducting nanwoire with a DNA molecule at its core. The DNA molecule play a role of a mechanical template. It is demonstrated that such nanowires can be used to make magnetic-field-sensitive quantum interferometers as well as samples that can be used to study the effect of macroscopic quantum tunneling.